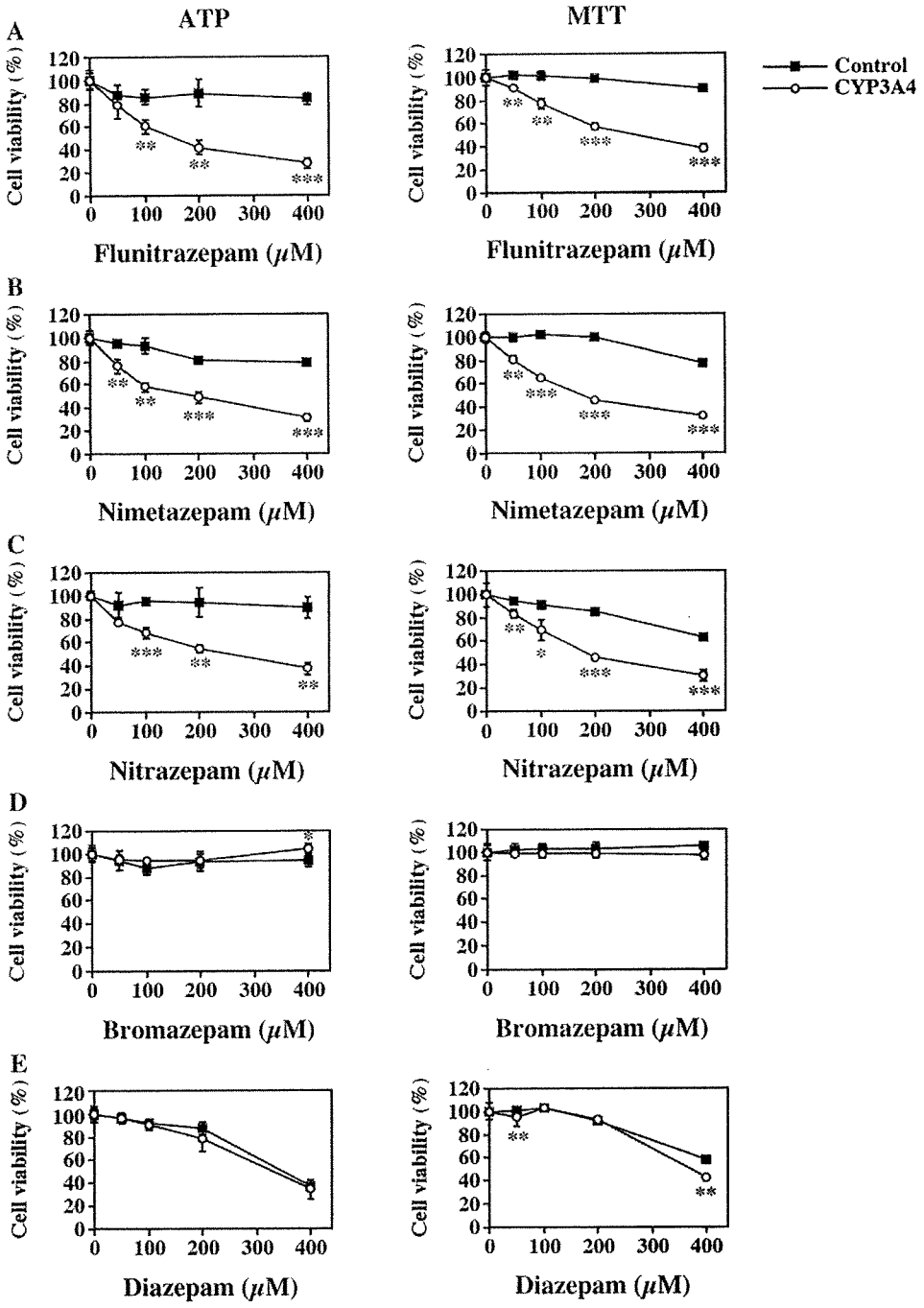

FIG. 2. Cytotoxicity of the benzodiazepines incubated with CYP3A4 on HepG2 cells. HepG2 cells seeded with the benzodiazepines and CYP3A4 or control Supersomes in 96-well plates were incubated at 37°C for 24 h. Cell viability was measured by ATP assay (left) and MTT assay (right) as described under *Materials and Methods*. The test compounds were flunitrazepam (A), nimetazepam (B), nitrazepam (C), bromazepam (D), and diazepam (E). Data represent the mean ± S.D. of three independent experiments. *, $P < 0.05$; **, $P < 0.01$; ***, $P < 0.001$, compared with the control Supersomes.

epam (data not shown). This finding suggested that the reactive metabolites of nitrobenzodiazepines may bind to glutathione. However, glutathione did not completely protect against the cytotoxicity; thus, there may be another cytotoxic effect that could not be detoxified by glutathione trapping.

In humans, the major metabolites of flunitrazepam are *N*-desmethylflunitrazepam in plasma and 3-hydroxyflunitrazepam and 7-aminoflunitrazepam in urine (Fukazawa et al., 1978). CYP3A4 is the major P450 involved in flunitrazepam 3-hydroxylation and *N*-desmethylation, but CYP2C9 and CYP2C19 also catalyze the *N*-desmethylation of flunitrazepam (Hesse et al., 2001; Kilicarslan et al., 2001). The reductive metabolite of flunitrazepam, 7-aminoflunitrazepam, is catalyzed by NADPH-cytochrome P450 reductase in HepG2 cells (Peng et al., 2004). Nimetazepam is metabolized to *N*-desmethylnimetazepam and 3-hydroxylnimetazepam (Dainippon Sumitomo Pharma, unpublished data). Nitrazepam is metabolized to 7-aminonitrazepam and 3-hydroxynitrazepam (Rieder, 1965). Although which P450 isoform mediates nimetazepam and nitrazepam metabolism has not been revealed, nimetazepam and nitrazepam may be metabolized by CYP2C9, CYP2C19, and CYP3A4. In our study, when HepG2 cells were exposed to 100 μM nitrobenzodiazepines, the differences in the cell viability between CYP2Cs and control Supersomes were less than 10% (Fig. 3), indicating that the contribution of CYP2Cs to the cytotoxicity of nitrobenzodiazepines was much lower than that of

DMD DRUG METABOLISM AND DISPOSITION aspet

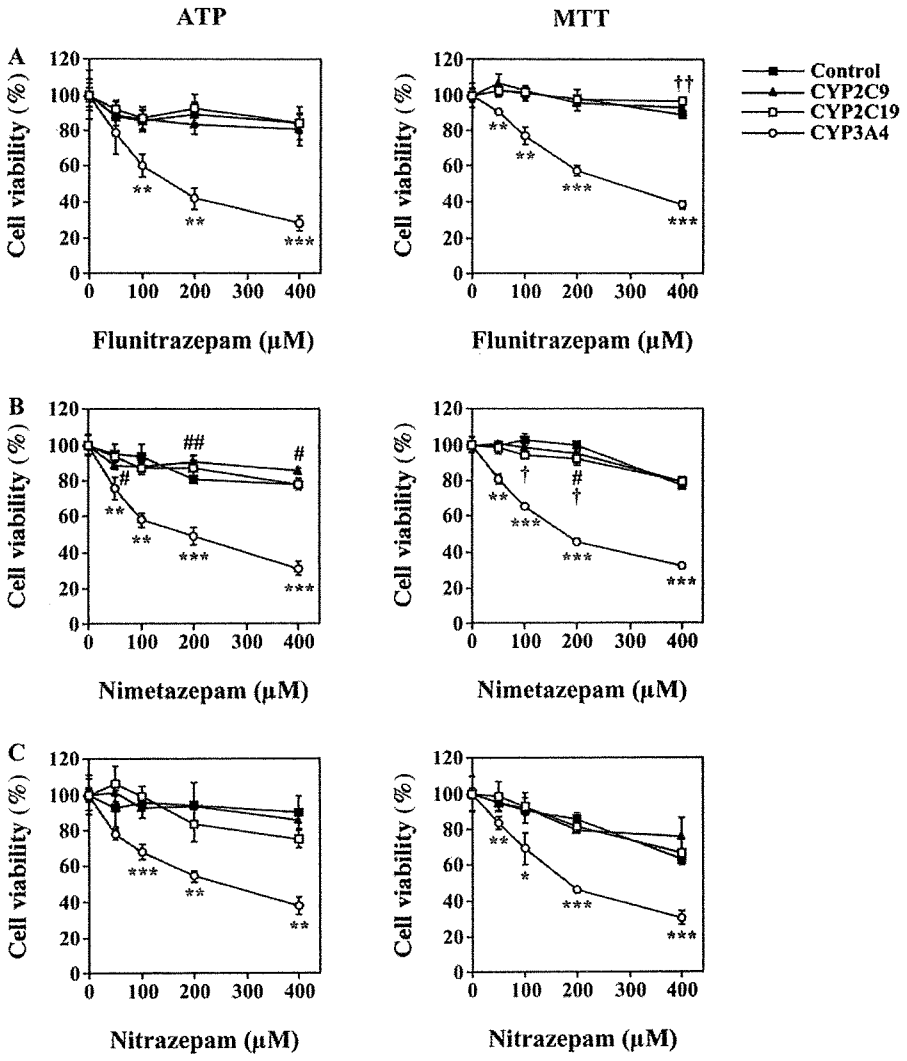

FIG. 3. Cytotoxicity of the benzodiazepines incubated with CYP2Cs in HepG2 cells. HepG2 cells seeded with the benzodiazepines and CYP2C9, CYP2C19, or control Supersomes in 96-well plates were incubated at 37°C for 24 h. Cell viability was measured by ATP assay (left) and MTT assay (right) as described under *Materials and Methods*. The test compounds were flunitrazepam (A), nimetazepam (B), and nitrazepam (C). Data for CYP3A4 and control Supersomes were redrawn from Fig. 2. Data represent the mean ± S.D. of three independent experiments. #, $P < 0.05$; ##, $P < 0.01$ (CYP2C9); †, $P < 0.05$; ††, $P < 0.01$ (CYP2C19); *, $P < 0.05$; **, $P < 0.01$; ***, $P < 0.001$ (CYP3A4), compared with the control Supersomes.

CYP3A4. Therefore, the metabolic activations of the nitrobenzodiazepines were CYP3A4-specific reactions.

Caspase 3 and 7 are classified as effector caspases. Active effector caspases mediate the cleavage of an overlapping set of protein substrates, resulting in the morphological features of apoptosis and the demise of the cell (Nuñez et al., 1998). Flunitrazepam, nimetazepam, and nitrazepam significantly increased the caspase 3/7 activities in HepG2 cells in the presence of CYP3A4 Supersomes (Fig. 4). Therefore, apoptosis after caspase 3 and 7 activation is one of the cytotoxic pathways of the reactive metabolites of flunitrazepam, nimetazepam, and nitrazepam.

The maximum plasma concentrations of nitrobenzodiazepines after a single administration in humans have been reported as follows: 0.04 μM after an oral dose of 2 mg of flunitrazepam (Fukazawa et al., 1978), 0.05 μM after an oral dose of 5 mg of nimetazepam (Dainippon Sumitomo Pharma, unpublished data), 0.3 μM after an oral dose of 10 mg of nitrazepam (Rieder, 1973), and 0.05 μM after an oral dose of 2 mg of clonazepam (Cavedal et al., 2007). Flunitrazepam was reported to induce hepatotoxicity by the Ministry of Health, Labor and Welfare of Japan, and nitrazepam and clonazepam were reported to cause drug-induced liver injury (Olsson and Zettergren, 1988; Seki et al., 2008). Although it is very difficult to extrapolate from an in vitro study to in vivo in humans, we may pay attention to the metabolic activation of nitrobenzodiazepines by CYP3A4.

The metabolism of a nontoxic drug to reactive metabolites is thought to initiate a variety of adverse reactions (Park, 1986; Parke, 1987). Glutathione is an important intracellular peptide that can detoxify reactive metabolites by conjugation (Lu, 1999). Previous studies reported that reactive metabolites of flutamide (Kang et al., 2007), trazodone (Kalgutkar et al., 2005), and troglitazone (Kassahun et al., 2001) formed by CYP3A4 were detoxified by glutathione conjugations. As shown in Fig. 5, glutathione adducts of flunitrazepam and nimetazepam were detected by LC-MS/MS, suggesting the production of reactive metabolites of flunitrazepam and nimetazepam catalyzed by CYP3A4. In the present study, the structure of the glutathione adduct of flunitrazepam was estimated by LCMS-IT-TOF as shown in Fig. 6. It seemed that a nitrogen atom in the side chain of flunitrazepam was conjugated with the thiol of glutathione. The structure of the glutathione adduct of nimetazepam may be similar to that of flunitrazepam because the fragment ions, $[M + H - 337]^+$ and $[M + H - 129]^+$, corresponded to those of flunitrazepam (Supplemental Fig. 3). The glutathione adducts of nitrazepam could not be detected either with or without CYP3A4 in our detection system. However, the cytotoxicity of nitrazepam to HepG2 cells treated with CYP3A4

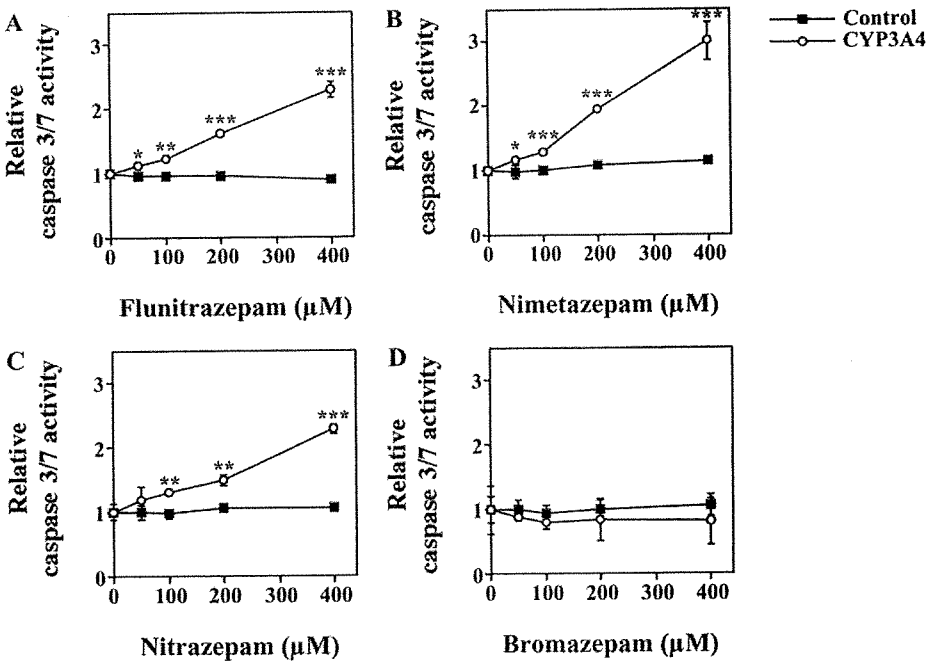

FIG. 4. Caspase 3/7 activity in HepG2 cells treated with CYP3A4 and the nitrobenzodiazepines. HepG2 cells in 96-well plates were incubated with benzodiazepines and CYP3A4 or control Supersomes at 37°C for 24 h. Caspase 3/7 activity was measured as described under *Materials and Methods*. The test compounds were flunitrazepam (A), nimetazepam (B), nitrazepam (C), and bromazepam (D). Data represent the mean ± S.D. of three independent experiments. *, $P < 0.05$; **, $P < 0.01$; ***, $P < 0.001$, compared with the control Supersomes.

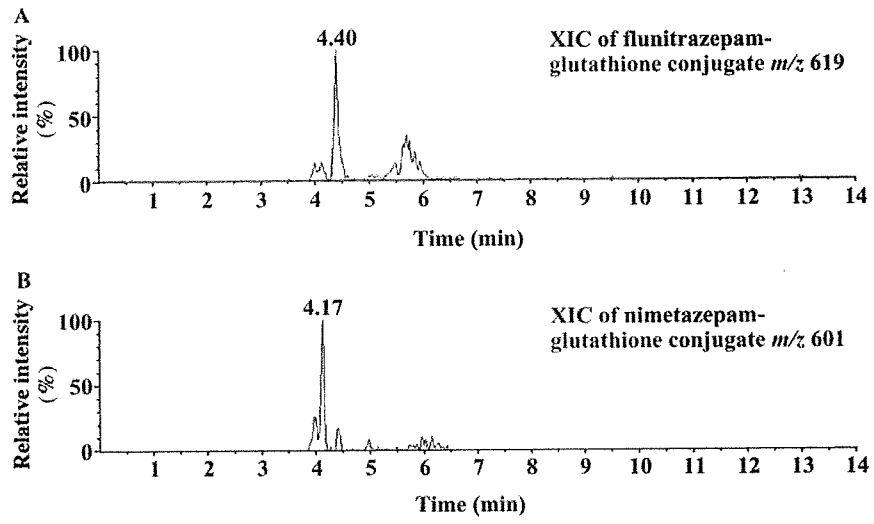

FIG. 5. Exacted ion chromatograms (XIC) of the glutathione adducts of benzodiazepines. The chromatograms were scanned with the precursor ion fragment, *m/z* 272, derived from glutathione using LC-MS/MS. A, flunitrazepam at *m/z* 619 ($[M - H]^-$); B, nimetazepam at *m/z* 601 ($[M - H]^-$).

Supersomes (Fig. 2) suggested that metabolic activation might occur. One of the reasons for this discrepancy may be the sensitivity of the detection.

Nitroaromatic drugs such as flutamide, nimesulide, and tolcapone have been associated with idiosyncratic liver injury (Boelsterli et al., 2006). In the reductive pathways from nitro to the fully reduced amine catalyzed by P450 and/or reductase, several reactive metabolites including nitroso and *N*-hydroxylamine derivatives could be produced. Such reactive metabolites seem to bind covalently to nucleophilic targets of proteins and nucleic acids, leading to the cytotoxic effects (Biaglow et al., 1986; Rickert, 1987; Kedderis and Miwa, 1988; Kedderis et al., 1989). On the other hand, arylamines are metabolically activated by P450-mediated *N*-hydroxylation. Electrophilic *N*-hydroxylamine reacts with intracellular molecules, which induce various types of toxicity including hepatotoxicity (Kato and Yamazoe, 1994). Flutamide induced severe hepatic dysfunction. Ohbuchi et al. (2008) suggested that CYP3A4 catalyzed the *N*-oxidation of the amino metabolite of flutamide, which had hepatotoxic effects. Although the bioactivation pathways of nitrobenzodiazepines still remain unclear, they may undergo metabolic activation similar to that of other drugs. Further study is needed to clarify the mechanism of metabolic activation concerning nitrobenzodiazepines.

In conclusion, we revealed that nitrobenzodiazepines, such as flunitrazepam, nimetazepam, and nitrazepam, were metabolically activated by CYP3A4, resulting in cytotoxicity in HepG2 cells. The CYP3A4 metabolites of flunitrazepam and nimetazepam were conjugated with glutathione at a nitrogen atom in the side chain. This finding suggested that metabolic activation by CYP3A4 may be one of the mechanisms in liver injury. Moreover, we established a simple assay system in which the cytotoxicity in HepG2 cells incubated with recombinant P450s and the drug was observed with high sensitivity. This assay system was useful for detecting metabolic activation by P450s and would be beneficial for predicting drug-induced cytotoxicity in preclinical drug development.

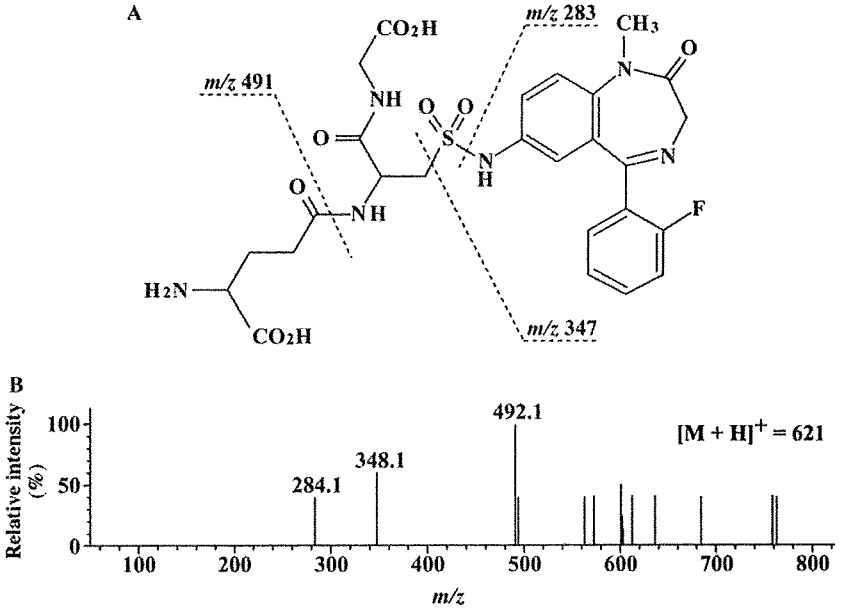

FIG. 6. A, predicted structure of the glutathione adduct of flunitrazepam. B, MS/MS spectra of the product ion obtained by collision-induced dissociation of the glutathione adduct of flunitrazepam at *m/z* 621 ([M + H]$^+$). These spectra were scanned using LCMS-IT-TOF.

Acknowledgments. We acknowledge Brent Bell for reviewing the article.

References

Berson A, Wolf C, Chachaty C, Fisch C, Fau D, Eugene D, Loeper J, Gauthier JC, Beaune P, and Pompon D (1993) Metabolic activation of the nitroaromatic antiandrogen flutamide by rat and human cytochromes P-450, including forms belonging to the 3A and 1A subfamilies. *J Pharmacol Exp Ther* **265:**366–372.

Biaglow JE, Varnes ME, Roizen-Towle L, Clark EP, Epp ER, Astor MB, and Hall EJ (1986) Biochemistry of reduction of nitro heterocycles. *Biochem Pharmacol* **35:**77–90.

Boelsterli UA, Ho HK, Zhou S, and Leow KY (2006) Bioactivation and hepatotoxicity of nitroaromatic drugs. *Curr Drug Metab* **7:**715–727.

Cavedal LE, Mendes FD, Domingues CC, Patni AK, Monif T, Reyar S, Pereira Ados S, Mendes GD, and De Nucci G (2007) Clonazepam quantification in human plasma by high-performance liquid chromatography coupled with electrospray tandem mass spectrometry in a bioequivalence study. *J Mass Spectrom* **42:**81–88.

Costa E, Auta J, Grayson DR, Matsumoto K, Pappas GD, Zhang X, and Guidotti A (2002) $GABA_A$ receptors and benzodiazepines: a role for dendritic resident subunit mRNAs. *Neuropharmacology* **43:**925–937.

Fukazawa H, Ichishita H, Honda M, and Shimazu H (1978) Pharmacokinetics studies of flunitrazepam in healthy male Japanese subjects. *Jpn J Clin Pharmacol Ther* **9:**251–265.

Guengerich FP (1995) Human cytochrome P-450 enzymes, in *Cytochrome P-450* (Ortiz de Montellano PR eds) pp. 473–535, Premium, New York.

Guengerich FP and Liebler DC (1985) Enzymatic activation of chemicals to toxic metabolites. *Crit Rev Toxicol* **14:**259–307.

Guengerich FP and MacDonald JS (2007) Applying mechanisms of chemical toxicity to predict drug safety. *Chem Res Toxicol* **20:**344–369.

Hesse LM, Venkatakrishnan K, von Moltke LL, Shader RI, and Greenblatt DJ (2001) CYP3A4 is the major CYP isoform mediating the in vitro hydroxylation and demethylation of flunitrazepam. *Drug Metab Dispos* **29:**133–140.

Hewitt NJ and Hewitt P (2004) Phase I and II enzyme characterization of two sources of HepG2 cell lines. *Xenobiotica* **34:**243–256.

Kalgutkar AS, Henne KR, Lame ME, Vaz AD, Collin C, Soglia JR, Zhao SX, and Hop CE (2005) Metabolic activation of the nontricyclic antidepressant trazodone to electrophilic quinone-imine and epoxide intermediates in human liver microsomes and recombinant P4503A4. *Chem Biol Interact* **155:**10–20.

Kang P, Dalvie D, Smith E, Zhou S, and Deese A (2007) Identification of a novel glutathione conjugate of flutamide in incubations with human liver microsomes. *Drug Metab Dispos* **35:**1081–1088.

Kassahun K, Pearson PG, Tang W, McIntosh I, Leung K, Elmore C, Dean D, Wang R, Doss G, and Baillie TA (2001) Studies on the metabolism of troglitazone to reactive intermediates in vitro and in vivo. Evidence for novel biotransformation pathways involving quinone methide formation and thiazolidinedione ring scission. *Chem Res Toxicol* **14:**62–70.

Kato R and Yamazoe Y (1994) Metabolic activation of *N*-hydroxylated metabolites of carcinogenic and mutagenic arylamines and arylamides by esterification. *Drug Metab Rev* **26:**413–429.

Kedderis GL, Argenbright LS, and Miwa GT (1989) Covalent interaction of 5-nitroimidazoles with DNA and protein in vitro: mechanism of reductive activation. *Chem Res Toxicol* **2:**146–149.

Kedderis GL and Miwa GT (1988) The metabolic activation of nitroheterocyclic therapeutic agents. *Drug Metab Rev* **19:**33–62.

Kilicarslan T, Haining RL, Rettie AE, Busto U, Tyndale RF, and Sellers EM (2001) Flunitrazepam metabolism by cytochrome P450s 2C19 and 3A4. *Drug Metab Dispos* **29:**460–465.

Lu SC (1999) Regulation of hepatic glutathione synthesis: current concepts and controversies. *FASEB J* **13:**1169–1183.

Nuñez G, Benedict MA, Hu Y, and Inohara N (1998) Caspases: the proteases of the apoptotic pathway. *Oncogene* **17:**3237–3245.

Ohbuchi M, Miyata M, Nagai D, Shimada M, Yoshinari K, and Yamazoe Y (2008) Role of enzymatic *N*-hydroxylation and reduction in flutamide metabolite-induced liver toxicity. *Drug Metab Dispos* **37:**97–105.

Olsson R and Zettergren L (1988) Anticonvulsant-induced liver damage. *Am J Gastroenterol* **83:**576–577.

Ono S, Hatanaka T, Miyazawa S, Tsutsui M, Aoyama T, Gonzalez FJ, and Satoh T (1996) Human liver microsomal diazepam metabolism using cDNA-expressed cytochrome P450s: role of CYP2B6, 2C19 and 3A subfamily. *Xenobiotica* **26:**1155–1166.

Park BK (1986) Metabolic basis of adverse drug reaction. *J R Coll Phys Lond* **20:**195–200.

Parke DV (1987) Activation mechanisms to chemical toxicity. *Arch Toxicol* **60:**5–15.

Peng FC, Chaing HH, Tang SH, Chen PC, and Lu SC (2004) NADPH-cytochrome P-450 reductase is involved in flunitrazepam reductive metabolism in HepG2 and Hep3B cells. *J Toxicol Environ Health A* **67:**109–124.

Rickert DE (1987) Metabolism of nitroaromatic compounds. *Drug Metab Rev* **18:**23–53.

Rieder J (1965) Methods for estimating 1,3-dihydro-7-nitro-5-phenyl-2*H*-1,4-benzodiazepin-2-one and its principal metabolites in biological samples and results of research on the pharmacokinetics and metabolism of this compound in humans and rats. *Arzneimittel-Forschung* **15:**1134–1148.

Rieder J (1973) Plasma levels and derived pharmacokinetic characteristics of unchanged nitrazepam in man. *Arzneimittel-Forschung* **23:**212–218.

Rodríguez-Antona C, Donato MT, Boobis A, Edwards RJ, Watts PS, Castell JV, and Gómez-Lechón MJ (2002) Cytochrome P450 expression in human hepatocytes and hepatoma cell lines: molecular mechanisms that determine lower expression in cultured cells. *Xenobiotica* **32:**505–520.

Schwartz MA, Koechlin BA, Postma E, Palmer S, and Krol G (1965) Metabolism of diazepam in rat, dog, and man. *J Pharmacol Exp Ther* **149:**423–435.

Seki E, Taniguchi H, Nagano R, Sakitani Y, Serizawa T, Ito Y, Mine N, Mizuno H, Mitsuno Y, and Nakata R (2008) Case report: severe hepatic disorder induced by chronic administration of antidepressants drugs. *552nd Meeting for the Japanese Society of Internal Medicine Kanto Division*: 2008 Mar 8; Tokyo, Japan. 31 p. The Japanese Society of Internal Medicine, Tokyo.

Shimada T, Yamazaki H, Mimura M, Inui Y, and Guengerich FP (1994) Interindividual variations in human liver cytochrome P-450 enzymes involved in the oxidation of drugs, carcinogens and toxic chemicals: studies with liver microsomes of 30 Japanese and 30 Caucasians. *J Pharmacol Exp Ther* **270:**414–423.

Uetrecht JP (1999) New concepts in immunology relevant to idiosyncratic drug reactions: the "danger hypothesis" and innate immune system. *Chem Res Toxicol* **12:**387–395.

Vignati L, Turlizzi E, Monaci S, Grossi P, Kanter R, and Monshouwer M (2005) An in vitro approach to detect metabolite toxicity due to CYP3A4-dependent bioactivation of xenobiotics. *Toxicology* **216:**154–167.

Wilkening S, Stahl F, and Bader A (2003) Comparison of primary human hepatocytes and hepatoma cell line HepG2 with regard to their biotransformation properties. *Drug Metab Dispos* **31:**1035–1042.

Yamamoto Y, Yamazaki H, Ikeda T, Watanabe T, Iwabuchi H, Nakajima M, and Yokoi T (2002) Formation of a novel quinone epoxide metabolite of troglitazone with cytotoxicity to HepG2 cells. *Drug Metab Dispos* **30:**155–160.

Address correspondence to: Dr. Tsuyoshi Yokoi, Drug Metabolism and Toxicology, Faculty of Pharmaceutical Sciences, Kanazawa University, Kakuma-machi, Kanazawa 920-1192, Japan. E-mail: tyokoi@kenroku.kanazawa-u.ac.jp

Biochemical Pharmacology 79 (2010) 288–295

Contents lists available at ScienceDirect

Biochemical Pharmacology

journal homepage: www.elsevier.com/locate/biochempharm

Transcriptional regulation of human carboxylesterase 1A1 by nuclear factor-erythroid 2 related factor 2 (Nrf2)☆

Taiga Maruichi, Tatsuki Fukami, Miki Nakajima, Tsuyoshi Yokoi *

Drug Metabolism and Toxicology, Faculty of Pharmaceutical Sciences, Kanazawa University, Kakuma-machi, Kanazawa 920-1192, Japan

ARTICLE INFO

Article history:
Received 21 July 2009
Accepted 19 August 2009

Keywords:
Carboxylesterase
Gene regulation
Nuclear factor-erythroid 2 related factor 2

ABSTRACT

Human carboxylesterase (CES) 1A, which is predominantly expressed in liver and lung, plays an important role in the hydrolysis of endogenous compounds and xenobiotics. CES1A is reported to be induced in human hepatocytes by butylated hydroxyanisole, ticlopidine and diclofenac, and the induction is assumed to be caused by oxidative stress. However, the molecular mechanism remains to be determined. In this study, we sought to investigate whether CES1A is regulated by nuclear factor-erythroid 2 related factor 2 (Nrf2), which is a transcriptional factor activated by oxidative stress, and clarify the molecular mechanism. Real-time reverse transcription-PCR assays revealed that CES1A1 mRNA was significantly induced by *tert*-butylhydroquinone (tBHQ) and sulforaphane (SFN), which are representative activators of Nrf2 in HepG2, Caco-2 and HeLa cells. The induction was completely suppressed with small interfering RNA for Nrf2. In HepG2 cells, the CES1A protein level and imidapril hydrolase activity, which is specifically catalyzed by CES1A, were also significantly induced by tBHQ and SFN. Luciferase assays revealed that the antioxidant response element (ARE) at −2025 in the *CES1A1* gene was responsible for the transactivation by Nrf2. In addition, electrophoretic mobility shift assays and chromatin immunoprecipitation assays revealed that Nrf2 binds to the ARE in the *CES1A1* gene. These findings clearly demonstrated that human CES1A1 is induced by Nrf2. This is the first study to demonstrate the molecular mechanism of the inducible regulation of human CES1A1.

1. Introduction

Human carboxylesterase (CES) is a member of serine hydrolase superfamily and involved in the hydrolysis of endogenous compounds and xenobiotics. In human, the CES1A and CES2 families play important roles in drug metabolism. The CES1A mainly hydrolyzes substrates with a small alcohol group and large acyl group, such as imidapril [1] and osertamivir [2]. In contrast, the CES2 prefers substrates with a large alcohol group and small acyl group, such as CPT-11 [3] and heroin [4]. Since CES1A has been reported to play roles as triglyceride hydrolase (TGH) [5], acyl coenzyme A:cholesterol acyltransferase (ACAT) [6] and cholesteryl ester hydrolase (CEH) [7], it seems probable that CES1A is important for the lipid metabolism as well as the drug metabolism. CES1A is predominantly expressed in liver and lung, whereas CES2 is expressed in colon and liver [8]. Human CES1A is classified into two isoforms, CES1A1 and CES1A2, with high homology at the mRNA level (99.3%). It has been accepted that the *CES1A2* gene is inverted and duplicated with the *CES1A1* gene [9]. However, we recently demonstrated that the *CES1A2* gene is a variant of the *CES1A3* pseudogene [10]. The sequence identity in the 5′-flanking region between the *CES1A1* and *CES1A2* genes is approximately 90% and the sequences downstream intron 1 of them are identical. Since only the N-terminal signal peptide sequences in exon 1 of CES1A1 and CES1A2 are different, mature proteins produced from both mRNA are identical. Our previous study revealed that the levels of CES1A1 mRNA transcribed from the *CES1A1* gene were substantially higher in liver than those of CES1A2 mRNA transcribed from the *CES1A2* gene [10]. Therefore, it is plausible that the level of CES1A1 mRNA rather than that of CES1A2 mRNA affects the level of mature protein and enzyme activity.

Cells are protected against oxidative stress by increasing the transcription of a group of genes coding antioxidant proteins and phase II enzymes, such as NAD(P)H:quinone oxidoreductase1 (NQO1) [11], heme oxigenase1 (HO-1) [12], and UDP-glucuronosyltransferase (UGT) 1A1 [13]. The most important regulator of the up-regulation is the transcription factor nuclear factor-erythroid 2 (NF-E2) related factor 2 (Nrf2). Nrf2 is a member of the cap'n'collar (CNC) family of transcriptional factors and contains a C-terminal basic leucine zipper structure that facilitates dimerization and DNA binding [14]. Nrf2 is highly expressed in detoxification tissues such as liver and kidney, and tissues that are exposed to the

☆ This study was supported by a Grant-in-Aid for Encouragement of Young Scientists of the Ministry of Education, Science, Sports and Culture #21790148.

* Corresponding author. Tel.: +81 76 234 4407; fax: +81 76 234 4407.
E-mail address: tyokoi@kenroku.kanazawa-u.ac.jp (T. Yokoi).

0006-2952/$ – see front matter © 2009 Elsevier Inc. All rights reserved.
doi:10.1016/j.bcp.2009.08.019

external environment, such as skin, lung and gastrointestinal tract [15]. In the absence of cellular stress, Nrf2 is localized in cytosol by binding with Kelch-like erythroid cell-derived protein with CNC homology (ECH)-associated protein 1 (Keap1), which acts as a substrate adopter for Cullin-dependent E3 ubiquitin ligase complex. Under the condition of oxidative stress, Nrf2 is released from Keap1 and translocates into the nucleus. After heterodimerization with small Maf protein, Nrf2 stimulates the transcription of the downstream genes by binding to antioxidant response element (ARE), a *cis*-acting enhancer with a consensus sequence defined as 5′-TMAnnRTGABnnnGCAwwww-3′, in which the core nucleotide is underlined [16,17]. *tert*-Butylhydroquinone (tBHQ) and sulforaphane (SFN) are known to be representative activators of Nrf2 [18].

There are few reports of the regulatory mechanism of human CES1A. Hosokawa et al. [19] demonstrated that Sp1 and C/EBP are involved in the basal expression of CES1A1. In addition, Nishimura et al. [20] reported that, in human hepatocytes, CES1A mRNA was not induced by rifampicin and omeprazole, which are potent ligands of pregnane X receptor and aryl hydrocarbon receptor (AhR), respectively. Thus, the inducible regulation of CES1A has not been reported until now. Recently, Takakusa et al. [21] reported that CES1A was induced by butylated hydroxyanisole, ticlopidine and diclofenac in human hepatocytes, and that the induction would be stimulated by oxidative stress. As described above, it is well known that Nrf2 is involved in the induction by oxidative stress. In addition, a computer-assisted homology search revealed putative AREs within −3200 bp of the *CES1A1* gene. Thus, it is plausible that Nrf2 is involved in the transcriptional regulation of CES1A. These lines of evidence prompted us to investigate whether the human *CES1A1* gene is regulated by Nrf2.

2. Materials and methods

2.1. Chemicals and reagents

tBHQ was purchased from Wako Pure Chemical Industries (Osaka, Japan). L-SFN was purchased from Alexis (San Diego, CA). Imidapril and imidaprilat were kindly supplied by Mitsubishi Tanabe Pharma Corporation (Osaka, Japan). Anti-human Nrf2 antibodies (C-20 and H-300), which recognize the C- and N-terminus of Nrf2 protein, respectively, were from Santa Cruz Biotechnology (Santa Cruz, CA). Stealth Select RNAi for Nrf2 (HSS107130) (5′-aaucacugaggccaaguaguguguc-3′) and Stealth RNAi negative control, Medium GC Duplex #2 were from Invitrogen (Carlsbad, CA). All primers and oligonucleotides were commercially synthesized at Hokkaido System Sciences (Sapporo, Japan). All other reagents were of the highest grade commercially available.

2.2. Cells and culture conditions

The human hepatoma cell line HepG2 and human colon carcinoma cell line Caco-2 were obtained from American Type Culture Collection (Manassas, VA). Human adenocarcinoma of the cervix of uterus cell line HeLa was obtained from RIKEN BioResource Center (Ibaraki, Japan). HeLa cells were cultured in Dulbecco's modified Eagle's medium (DMEM) (Nissui Pharmaceutical, Tokyo, Japan) supplemented with 10% fetal bovine serum (FBS) (Invitrogen). HepG2 and Caco-2 cells were cultured in DMEM supplemented with 10% FBS and 0.1 mM nonessential amino acids (Invitrogen). The cells were maintained at 37 °C under an atmosphere of 5% CO_2.

2.3. Real-time reverse transcription (RT)-polymerase chain reaction (PCR) analysis

Total RNA was extracted using RNAiso (Takara Bio, Shiga, Japan) and cDNA was synthesized from total RNA using ReverTra Ace (TOYOBO, Osaka, Japan) according to the manufacturer's protocol. Human GAPDH mRNA was quantified by real-time RT-PCR using the Smart Cycler (Cepheid, Sunnyvale, CA) as described previously [22]. CES1A1, CES2 and HO-1 mRNA levels were quantified under the same condition. PCR was performed with the following primer sets: CES1A1, CES1A1 S and CES1A1 AS; CES2, CES2 S and CES2 AS; HO-1, HO-1 S and HO-1 AS (Table 1).

Table 1
Sequences of oligonueleotide used in the present study.

Oligonucleotide	Sequence
For real-time RT-PCR	
CES1A1 S[a]	5′-atgtggctccgtgcct-3′
CES1A1 AS[a]	5′-tcttcacaaagctccatggt-3′
CES2 S[b]	5′-aacctgtctgcctgtgaccaagt-3′
CES2 AS[b]	5′-acatcagcagcgttaacattttctg-3′
HO-1 S[c]	5′-atagagcgaaacaagcaga-3′
HO-1 AS[c]	5′-tagagctgtttgaacttgg-3′
GAPDH S[d]	5′-ccagggctgcttttaactc-3′
GAPDH AS[d]	5′-gctcccccctgcaaatga-3′
For SOE-PCR	
pGL3 S	5′-tagcaaaataggctgtcccc-3′
pGL3 AS	5′-tcgatatgtgcatctgtaaaa-3′
ARE2 mt-A	5′-atctaaggcaaattTTCTTGTCAgctcatt-3′
ARE2 mt-B	5′-aatgagcTGACAAGAAaatttgccttagat-3′
ARE3 mt-A	5′-acagcaactcaatgTTAAAGTCAgaaccag-3′
ARE3 mt-B	5′-ctggttcTGACTTTAAcattgagttgctgt-3′
ARE4 mt-A	5′-cccgtgagattaatTTTGTCTCAcgatctt-3′
ARE4 mt-B	5′-aagatcgTGAGACAAAattaatctcacggg-3′
For ChIP assays	
CES1A1 −2178 S	5′-gaccttaggcaatccctcct-3′
CES1A1 −1855 AS	5′-tggctgtaatcttgtcagtgtttc-3′
CES1A1 −1274 S	5′-tctttgtgtacaagcttttgtg-3′
CES1A1 −956 AS	5′-cacaaggaagtcactcaaag-3′
CES1A1 −958 S	5′-gtgtccccagcagcttgtaa-3′
CES1A1 −666 AS	5′-aaaatgaactccgtccccccc-3′
For electrophoresis mobility shift assays	
cARE[e]	5′-gatcttttatgctgagtcatggttt-3′
CES1A1 ARE4	5′-atttaagatcgTGAGACAGCattaatctc-3′
CES1A1 ARE4mt	5′-atttaagatcgTGAGACAAAattaatctc-3′
CES1A1 ARE6	5′-taggggaattGCTGGGTCAtatggaaactc-3′
CES1A1 ARE6mt	5′-taggggaattTTTGGGTCAtggaaactc-3′

The core ARE is indicated by capital letters and mutated nucleotides are underlined.
[a] From Fukumi et al. [10].
[b] From Sanghani et al. [23].
[c] From Nakamura et al. [24].
[d] From Tsuchiya et al. [22].
[e] From Balogun et al. [12].

2.4. Immunoblot analysis

The expression of CES1A protein was measured by SDS-polyacrylamide gel electrophoresis and immunoblot analysis according to Laemmli [25]. For the preparation of cell homogenates, HepG2 cells were suspended in TGE buffer (10 mM Tris–HCl (pH 7.4), 20% glycerol, 1 mM EDTA) and disrupted by freeze–thawing three times. The protein concentrations were determined according to Bradford [26]. Cell homogenates (30 μg) were separated on 7.5% polyacrylamide gels and electrotransferred onto polyvinylidene difluoride membrane, Immobilon-P (Millipore, Billerica, MA). The membranes were probed with polyclonal rabbit anti-human CES1A (Abcam, Cambridge, MA), and IRDye680-labeled anti-rabbit IgG and an Odyssey infrared imaging system (LI-COR Biosciences, Lincoln, NE) were used for detection. The relative expression level was quantified using ImageQuant TL Image Analysis software (GE Healthcare, Buckinghamshire, UK).

2.5. Imidapril hydrolase activity

The imidapril hydrolase activity was determined according to the method described previously with a slight modification [27]. A

typical standard reaction mixture (total volume, 0.2 ml) contained HepG2 cell homogenates (1 mg/ml), 100 mM Tris–HCl buffer (pH 7.4) and 100 μM imidapril. The final concentration of the organic solvent in the reaction mixture was <1.0%. The reaction was initiated by the addition of imidapril after 2 min of preincubation at 37 °C. After 30 min of incubation, the reaction was terminated by adding 100 μl of ice-cold acetonitrile. After the removal of protein by centrifugation at 9500 × *g* for 5 min, a 10 μl portion of the supernatant was subjected to liquid chromatography-tandem mass spectrometry with an Inertsil ODS-3 analytical column (2.1 mm × 100 mm; GL Science, Tokyo, Japan). The mobile phase consisted of acetonitrile/10 mM ammonium formate (20:80). The mass/charge (*m/z*) ion transitions were recorded in the multiple reaction monitoring mode: *m/z* 378.2 and 206.3 for imidaprilat.

2.6. Construction of reporter plasmid

A pGL3 plasmid containing two copies of the consensus ARE (2× cARE) in the human *NQO-1* gene (5′-gatcagtcacagtgactcagcagaatct-3′), which was previously constructed in our laboratory [24], was used as a positive control. The PCR fragments of the 5′-flanking region (−3207 to −1 bp) in the *CES1A1* gene amplified using genomic DNA samples were cloned into the pGL3-basic vector (Promega, Madison, MI) after treatment with Klenow Fragment (Takara) and digestion with *Xho* I. This plasmid (−3207 to −1 bp) was used for construction of the other reporter plasmids (−1531 to −1, and −833 to −1 bp) by digestion and subcloning. Throughout this article, base A in the initiation codon ATG is denoted +1 and the base before A is numbered −1. Three reporter plasmids containing ARE(s), the −3041 to −2891 bp plasmid that contained ARE1, the −2365 to −1989 bp plasmid that contained ARE2, ARE3 and ARE4, and the −1310 to −1170 bp plasmid that contained ARE5 and ARE6 were constructed by PCR and subcloning. The plasmids mutated at the AREs (ARE2 mt, ARE3 mt and ARE4 mt) were constructed by splicing with overlap extension (SOE)–PCR [28]. The regions around the nucleotides to be mutated were amplified using primer pairs pGL3 S and mt-A (PCR 1), or mt-B and pGL3 AS (PCR 2) (Table 1). The following SOE–PCR was performed with the primer pair pGL3 S and pGL3 AS, combining the PCR products 1 and 2. The SOE–PCR products were digested with the appropriate restriction enzymes and subcloned into the pGL3-tk vector. The nucleotide sequences were confirmed by DNA sequence analysis (Long-Read Tower DNA sequencer; GE Healthcare).

2.7. Transfection and luciferase assay

For siRNA transfection, HepG2, Caco-2 and HeLa cells were transfected with 30 pmol siRNA by using lipofectamine RNAiMAX (Invitrogen). After incubation for 24 h, the cells were treated with 80 μM tBHQ, 10 μM SFN or 0.1% dimethyl sulfoxide (DMSO) for 24 h. For the luciferase assays, HepG2 cells were seeded into 24-well plates at 1×10^5 cells/well. Transfection was performed using Tfx-20 reagent (Promega). The transfection mixtures consisted of 200 ng of pGL3 plasmid, 10 ng of phRL-TK plasmid (Promega), and 100 ng of human Nrf2 expression plasmid [24] or pTARGET empty plasmid as a control. The cells were harvested 48 h after transfection and lysed to measure the luciferase activity using a Dual Luciferase Reporter Assay System (Promega). The relative luciferase activities were normalized with the *Renilla* luciferase activities.

2.8. Electrophoretic mobility shift assay (EMSA)

Double-stranded oligonucleotides were labeled with [γ-^{32}P]ATP using T4 polynucleotide kinase (TOYOBO) and purified by Microspin G-50 columns (GE Healthcare). The oligonucleotide sequences are shown in Table 1. The labeled probe (40 fmol, ~20,000 cpm) was applied to each binding reaction in 25 mM HEPES-KOH (pH 7.9), 0.5 mM EDTA (pH 8.0), 10% glycerol, 50 mM KCl, 0.5 mM dithiothreitol, 0.5 mM (*p*-amidinophenyl)methanesulfonyl fluoride, 1 μg of poly(dI-dC), 5 μg of salmon sperm DNA, and 8 μg of the nuclear extracts from 0.1% DMSO- or 10 μM SFN-treated HepG2 cells prepared using NE-PER Nuclear and cytoplasmic extraction reagents (Pierce, Rockford, IL) with a final reaction volume of 15 μl. To determine the specificity of the binding to the oligonucleotides, competition experiments were conducted by co-incubation with 5-, 25-, and 50-fold excesses of unlabeled competitors. For supershift experiments, 2 μg of anti-Nrf2 antibodies (C-20 and H-300) or normal rabbit IgG were preincubated with the nuclear protein on ice for 30 min. The reactions were incubated on ice for 15 min and then loaded on 4% acrylamide gel in 0.5× Tris–borate EDTA buffer. The gels were dried and exposed to film for 24 h. The DNA–protein complexes were detected with a Fuji Bio-Imaging Analyzer BAS 1800 (Fuji Film, Tokyo, Japan).

2.9. Chromatin immunoprecipitation (ChIP) assay

When HepG2 cells reached 60% confluence in 60-mm dishes, they were treated with 0.1% DMSO or 10 μM SFN. After 24 h incubation, ChIP assays were performed using a ChIP assay kit (Upstate, Lake Placid, NY) according to the manufacturer's protocol. Rabbit anti-Nrf2 antibodies (C-20 and H-300) and normal rabbit IgG were used for immunoprecipitation of the protein–DNA complexes. PCR was performed with the following primer sets: region 1, CES1A1 −2178 S and CES1A1 −1855 AS; region 2, CES1A1 −1274 S and CES1A1 −956 AS; region 3, CES1A1 −956 S and CES1A1 −666 AS (Table 1). The PCR conditions were as follows: after initial denaturation at 94 °C for 3 min, the amplification was performed by denaturation at 94 °C for 25 s, annealing at 58 °C (region 1), 54 °C (region 2) or 60 °C (region 3) for 25 s, and extension at 72 °C for 30 s for 30 cycle. The PCR products were electrophoresed on a 2% agarose gel and visualized by ethidium bromide.

2.10. Statistical analysis

Data are expressed as mean ± SD. Statistical significance between two groups was determined by two-tailed Student's *t*-test. Statistical significance between multiple groups was determined by ANOVA followed by Dunnett or Tukey test. A value of $P < 0.05$ was considered statistically significant.

3. Results

3.1. Induction of CES1A in cultured cells

The effects of tBHQ and SFN on the expression of CES1A1 mRNA in HepG2, Caco-2 and HeLa cells were examined (Fig. 1). By treatment with 80 μM tBHQ and 10 μM SFN, the expression of CES1A1 mRNA was significantly increased in HepG2 (2.6- and 3.4-fold, respectively), Caco-2 (3.4- and 4.4-fold) and HeLa cells (3.4- and 3.0-fold). Under the same condition, the level of HO-1 mRNA, which is already known to be induced by Nrf2, was also significantly induced in all cell lines. In contrast, the level of CES2 mRNA was not changed in any of cell lines. The CES1A protein expression and enzyme activity were measured to examine whether they were increased by the induction of CES1A1 mRNA expression by tBHQ and SFN in HepG2 cells. Immunoblot analysis revealed that the expression of CES1A protein was clearly increased up to 1.73- and 2.12-fold in HepG2 cells by tBHQ and SFN, respectively (Fig. 1B). In Caco-2 and HeLa cells, it was difficult to detect CES1A protein by immunoblot analysis due to the

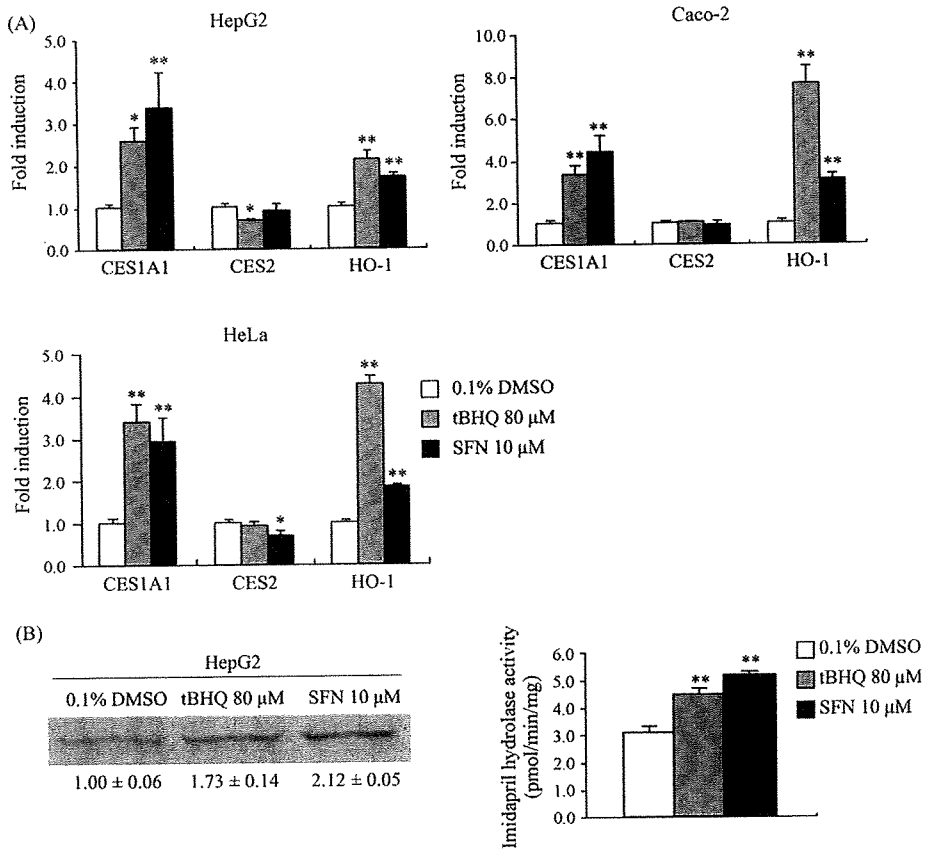

Fig. 1. (A) Effects of tBHQ and SFN on the CES1A1, CES2 and HO-1 mRNA expression in HepG2, Caco-2, and HeLa cells. The cells were treated with 80 μM tBHQ, 10 μM SFN or DMSO vehicle (0.1%) for 24 h. The expressions of CES1A1, CES2 and HO-1 mRNA were determined by real-time RT-PCR and normalized with the GAPDH mRNA levels. Effects of tBHQ and SFN on the expression of CES1A protein (B) and the imidapril hydrolase activity (C) in HepG2 cells. The cells were treated with 80 μM tBHQ, 10 μM SFN or DMSO vehicle (0.1%) for 24 h. The expression of CES1A protein was determined by immunoblot analysis. Each column represents the mean ± SD of three independent experiments. $^{*}P < 0.05$; $^{**}P < 0.01$ compared with control (vehicle).

low expression level. Imidapril hydrolase activity, which is specifically catalyzed by CES1A, was also significantly increased in HepG2 cells by tBHQ and SFN (from 3.4 ± 0.23 to 4.13 ± 0.23 and 5.31 ± 0.15 pmol/min/mg protein, respectively) (Fig. 1C). These results indicate that the induction of CES1A1 mRNA expression by tBHQ and SFN led to increases in CES1A protein expression and enzyme activity.

3.2. Effect of Nrf2 knockdown on the induction of CES1A1 by tBHQ and SFN

To investigate whether Nrf2 is responsible for the induction of CES1A1 by tBHQ and SFN, the endogenous Nrf2 was knockdowned in HepG2, Caco-2 and HeLa cells (Fig. 2). It was confirmed that the Nrf2 mRNA expression was decreased 79%, 82%, and 88% by siRNA-Nrf2 transfection in HepG2, Caco-2, and HeLa cells, respectively. In all cell lines, tBHQ and SFN mediated induction of CES1A1 mRNA was completely suppressed by the knockdown of Nrf2. In HepG2 and Caco-2 cells, the basal expression level of CES1A1 mRNA was not changed by siRNA-Nrf2 transfection, whereas it was significantly decreased in HeLa cells. These results suggested that Nrf2 plays a critical role in the induction of CES1A1 by tBHQ and SFN.

3.3. Identification of Nrf2 binding site in the 5′-flanking region of the CES1A1 gene

A computer-assisted homology search identified six putative AREs within −3200 bp of the *CES1A1* gene (Fig. 3). These AREs at −2971, −2323, −2203, −2025, −1283, and −1218 bp were termed ARE1, ARE2, ARE3, ARE4, ARE5 and ARE6, respectively. To investigate whether AREs in the *CES1A1* gene were functional in Nrf2-dependent transactivation, luciferase assays were performed using reporter plasmids containing the 5′-flanking region of the *CES1A1* gene (−3207 to −1, −1531 to −1, and −833 to −1 bp) in HepG2 cells (Fig. 4A). The transcriptional activity of 2× cARE used as positive control was increased up to 2.2-fold by the overexpression of Nrf2. Unexpectedly, the overexpression of Nrf2 did not activate the transcriptional activities of any plasmids. Then, we constructed three reporter plasmids containing ARE-neighboring regions and luciferase assays were performed (Fig. 4B). The transcriptional activities of the −2365 to −1989 bp plasmid that contained ARE2, ARE3 and ARE4 were increased up to 2.0-fold by the overexpression of Nrf2. In contrast, Nrf2 did not activate the transcriptional activities of the −3041 to −2891 bp plasmid that contained ARE1 and the −1310 to −1170 bp plasmid that contained ARE5 and ARE6. To further confirm the functional ARE, a mutation was introduced into each ARE of the −2365 to −1989 bp plasmid. The Nrf2-dependent transcriptional activation with the −2365 to −1989 bp plasmid was completely abolished by introducing the mutation in ARE4 (Fig. 4C). These results suggest that the ARE4 works as a functional Nrf2 response element in the *CES1A1* gene.

3.4. Nrf2 directly binds to the ARE at −2025 of the CES1A1 gene

To examine whether Nrf2 directly binds to ARE4, EMSA was performed using the nuclear extract prepared from DMSO- or SFN-treated HepG2 cell and ^{32}P-labeled ARE4 as a probe (Fig. 5). When

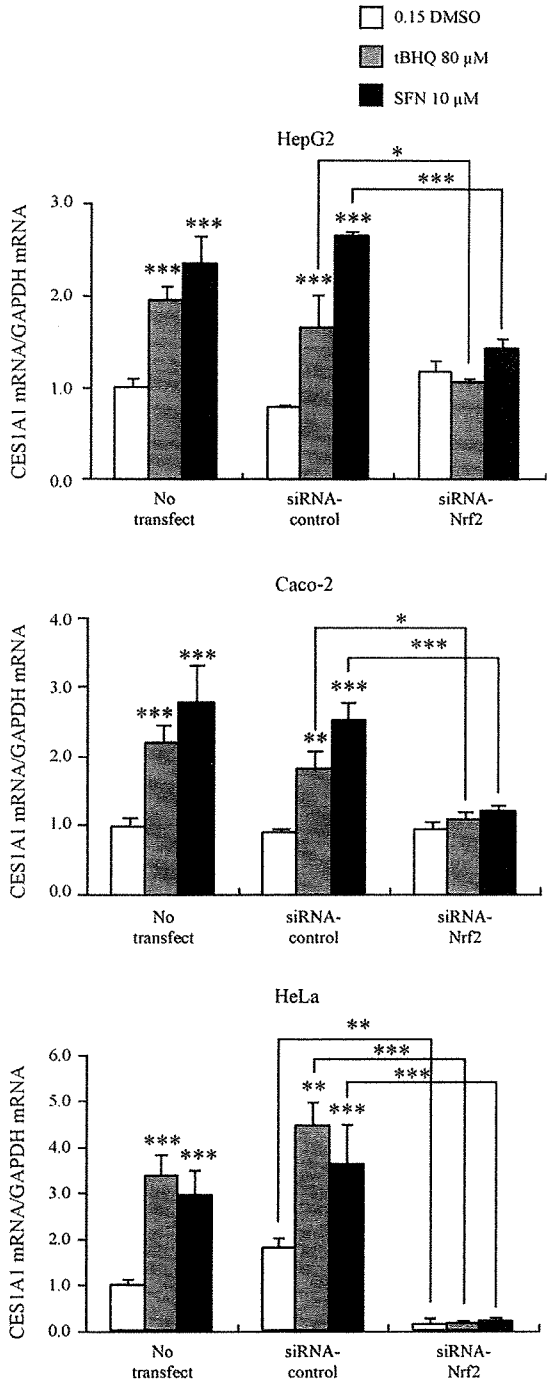

Fig. 2. Effect of Nrf2 knockdown on CES1A1 mRNA induction in HepG2, Caco-2 and HeLa cells. The expression of CES1A1 mRNA was determined by real-time RT-PCR. After 24 h transfection with siRNA, the cells were treated with 80 μM tBHQ, 10 μM SFN or DMSO vehicle (0.1%) for 24 h. To normalize RNA loading and PCR variations, the CES1A1 mRNA levels were corrected with the GAPDH mRNA levels. Each column represents the mean ± SD of three independent experiments. $^{*}P < 0.05$; $^{**}P < 0.01$; $^{***}P < 0.001$ compared with control (vehicle).

the probe was incubated with the nuclear extracts from the SFN-treated HepG2 cells, the shifted band was clearly observed. The band density was diminished with both anti-Nrf2 antibodies (C-20 and H-300), although the supershifted band was observed only with the anti-Nrf2 antibody (C-20). These results indicate that the shifted band contained Nrf2 complexes. Moreover, the shifted

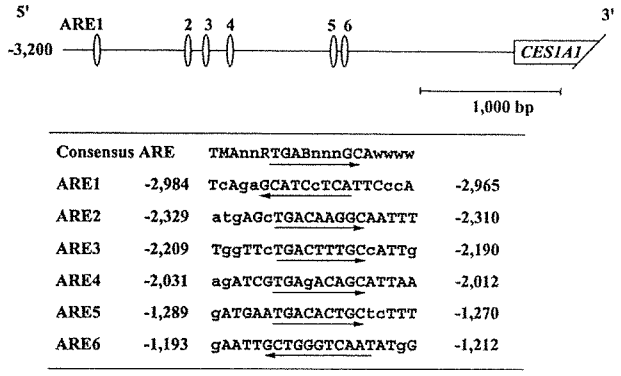

Consensus ARE		TMAnnRTGABnnnGCAwwww	
ARE1	-2,984	TcAgaGCATCcTCATTCccA	-2,965
ARE2	-2,329	atgAGcTGACAAGGCAATTT	-2,310
ARE3	-2,209	TggTTcTGACTTTGCcATTg	-2,190
ARE4	-2,031	agATCGTGAgACAGCATTAA	-2,012
ARE5	-1,289	gATGAATGACACTGCtcTTT	-1,270
ARE6	-1,193	gAATTGCTGGGTCAATATgG	-1,212

Fig. 3. Schematic diagram of putative AREs in the 5′-flanking region of the human *CES1A1* gene. Numbers indicate the nucleotide position when the A in the initiation codon ATG is denoted +1 and the base before A is numbered −1. The core ARE sequence is indicated by an arrow. The nucleotides that are consistent with the consensus ARE are shown with capital letters.

band was competed out by excess amounts of unlabeled cARE or ARE4, but not by the mutant ARE, ARE4 mt. These results suggested that Nrf2 binds to the ARE located at −2025 in the 5′-flanking region of the *CES1A1* gene.

To further examine whether Nrf2 binds to ARE4 in intact cells, ChIP assays were performed using DMSO- or SFN-treated HepG2 cells (Fig. 6). PCR was performed with primers designed to amplify the −2178 to −1855 bp (region 1) containing ARE4, the −1274 to −956 bp (region 2) containing ARE6 and the −958 to −666 bp (region 3) containing no AREs. Normal rabbit IgG was used as a negative control of immunoprecipitation for ChIP assays. As shown in Fig. 6, the immunoprecipitants of SFN-treated HepG2 cells obtained with anti-Nrf2 antibody (C-20) generated a distinct PCR product for region 1, but those obtained with anti-Nrf2 antibody (H-300) or normal rabbit IgG did not. Using primer sets for region 2 and region 3, no PCR products were obtained with any antibodies. These results suggest that Nrf2 binds to the ARE located at −2025 in the 5′-flanking region of the *CES1A1* gene in intact cells.

4. Discussion

In this study, we demonstrated that human CES1A1 is induced by Nrf2. The human *CES1A1* gene and *CES1A3* pseudogene are inverted and duplicated genes. Our recent study demonstrated that the *CES1A2* gene is a variant of the *CES1A3* pseudogene [10]. In the present study, we demonstrated that the ARE4 in the *CES1A1* gene was the key element of Nrf2-mediated induction, but the sequence of the region corresponding to ARE4 in the *CES1A1* gene exists in the *CES1A2* gene. Therefore, it is conceivable that CES1A2 mRNA derived from the *CES1A2* gene is also induced by Nrf2. The copy numbers of the *CES1A2* gene and *CES1A3* pseudogene were investigated for HepG2, Caco-2 and HeLa cells according to Fukami et al. [10] (data not shown). HepG2 and Caco-2 cells had two copies of the *CES1A3* gene, but HeLa cells had one copy each of the *CES1A3* and *CES1A2* genes. However, in HeLa cells, CES1A2 mRNA was not detected (data not shown), thus the induction of CES1A2 by Nrf2 could not be further investigated. Since the expression of CES1A2 mRNA is much lower than that of CES1A1 mRNA in human liver [10], the Nrf2-mediated induction of CES1A2 would have a minor effect on the CES1A enzyme activity.

NQO1, HO-1, and UGT1A1 are well known to be induced by tBHQ and SFN via Nrf2 [11–13]. Recently, these inductions have attracted attention as biomarkers of the electrophilic stress caused by the formation of reactive metabolites because they serve as a cellular defense against electrophiles and oxidative stress products [29]. It is plausible that CES1A1 is also a possible biomarker of

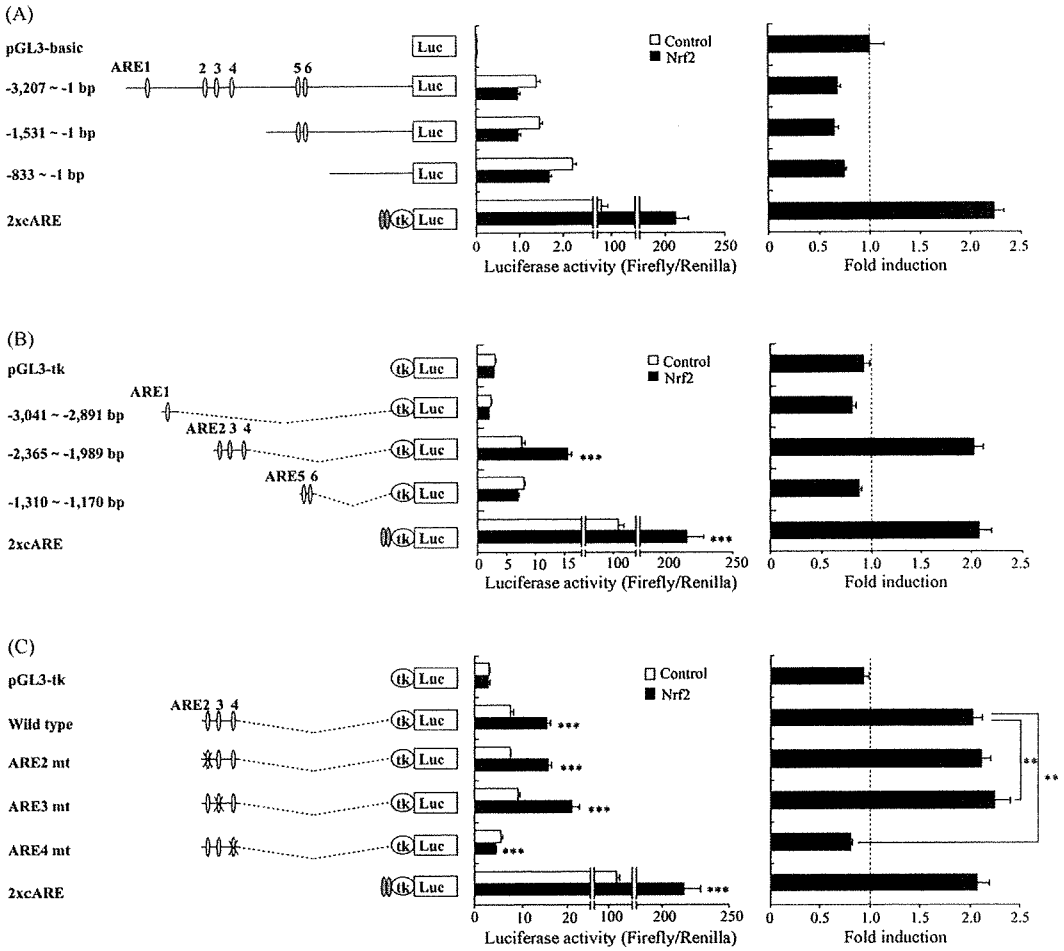

Fig. 4. Relative promoter activity of constructs containing putative ARE(s) in the 5′-flanking region of the *CES1A1* gene and the effect of the overexpression of Nrf2 in HepG2 cells. After 48 h transfection, the cells were harvested and assayed for the luciferase activities according to the manufacturer's protocol. The relative luciferase activities were normalized with the *Renilla* luciferase activities. The right part of the figure shows the fold induction of the transcriptional activity by the overexpression of Nrf2. Each column represents the mean ± SD of three independent experiments. 2×cARE indicates the plasmid containing two copies of the consensus ARE in the human NQO-1 gene. ARE2 mt, AER3 mt, ARE4 mt indicate the plasmids mutated at the ARE2, ARE3, and ARE4, respectively. Control, pTARGET empty plasmid. $^{**}P < 0.01$ and $^{***}P < 0.001$.

electrophilic stress because it was demonstrated in this study that CES1A1 is induced by Nrf2. tBHQ and SFN are also known as ligands of AhR [30,31]. NQO1, HO-1, and UGT1A1 are induced by AhR as well as by Nrf2 [32–34]. In the present study, CES1A1 induction by tBHQ and SFN was completely suppressed by knockdown of Nrf2. In addition, it was reported that CES1A mRNA is not induced by omeprazole, a potent ligand of AhR, in human hepatocytes [20]. These results indicate that only Nrf2 but not AhR would be involved in the CES1A1 induction by tBHQ and SFN. Interestingly, in HeLa cells, the basal expression level of CES1A1 mRNA was significantly decreased by the knockdown of Nrf2. This result indicates that Nrf2 regulates the basal expression of CES1A1 in HeLa cells. Similarly, it was reported that the basal expression level of carboxylesterase in lung and small intestine is decreased in Nrf2 knockout mice [35,36]. In addition to Sp1 and C/EBP [19], Nrf2 might also regulate the basal expression level of CES1A1.

Generally, the genes induced by Nrf2 are involved in detoxification [18]. Because CES1A expression was induced by Nrf2, it was conceivable that CES1A is also involved in detoxification. It was reported that carboxylesterase in human lung microsomes, in which CES1A is highly expressed, is involved in the detoxification of vinyl carbamate [37]. To our knowledge, this is the only report suggesting the involvement of CES1A in the detoxification of reactive intermediates and carcinogens. It appears that CES1A is associated with lipid elimination in the liver [4–6]. Oxidative stress is one of the causal factors for hepatic steatosis, which leads to liver injury [38]. Although there were no reports about the relevance of CES1A to hepatic steatosis, CES1A may be involved in the defense of the cells against hepatic steatosis.

As shown in Fig. 4B, the transcriptional activities using the plasmid containing sequence −2365 to −1989 in the 5′-flanking region of the *CES1A1* gene were increased up to 2.0-fold by overexpression of Nrf2, and it was demonstrated that the ARE4 works as a functional Nrf2 response element in the *CES1A1* gene. Although we analyzed the transcriptional activity using plasmids containing the sequences −3207 to −1, −1531 to −1, and −833 to −1 bp in the 5′-flanking region of the *CES1A1* gene, the activity was not increased by the overexpression of Nrf2 (Fig. 4A). This result was similar to that in our previous study in which a significant increase of the transcriptional activity by Nrf2 overexpression was not observed using plasmids containing the sequences −2191 or −1408 to −7 in the 5′-flanking region of the *UGT2B7* gene [24]. It is assumed that the plasmid containing the long sequence results in a complicated conformation, which makes it difficult for Nrf2 to bind to the target ARE.

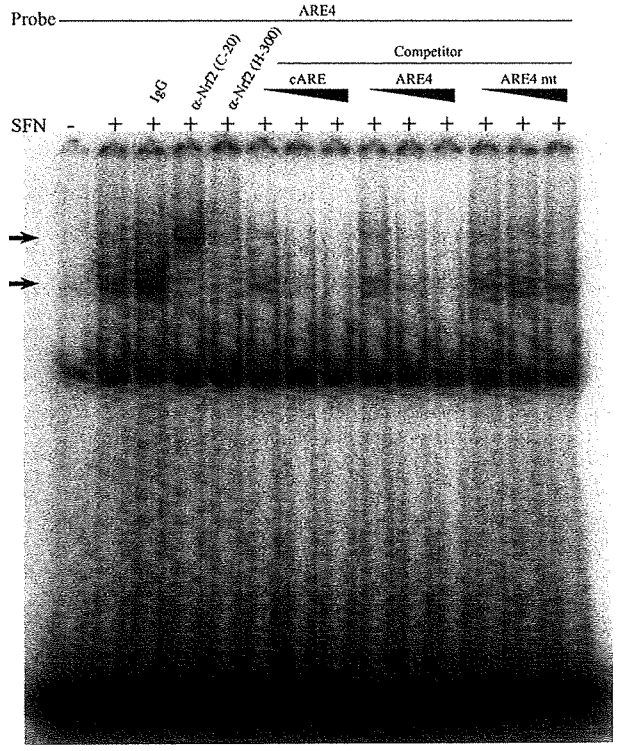

Fig. 5. Electrophoretic mobility shift assays of Nrf2 binding to ARE4 in the *CES1A1* gene. Oligonucleotide probes of CES1A1 ARE4 labeled with ^{32}P were incubated with nuclear extracts prepared from HepG2 cells treated with 10 μM SFN or DMSO vehicle (0.1%). The sequences of the oligonucleotides are shown in Table 1. Cold oligonucleotides were used as a competitor at 5-, 25-, and 50-fold molar excess. For supershift analyses, 2 μg of anti-Nrf2 antibodies (α-Nrf2) or normal rabbit IgG (IgG) were preincubated with the nuclear extracts on ice for 30 min. The *lower* arrow indicates the position of the Nrf2-dependent shifted band, and the *upper* one indicates the supershifted complex by anti-Nrf2 antibodies.

EMSA and ChIP assays revealed that Nrf2 binds to the 5′-flanking region in the *CES1A1* gene (Figs. 5 and 6). In EMSA, the supershifted band was observed only with the anti-Nrf2 antibody (C-20) but not with the anti-Nrf2 antibody (H-300). This result is consistent with our previous study [24]. In ChIP assays, the

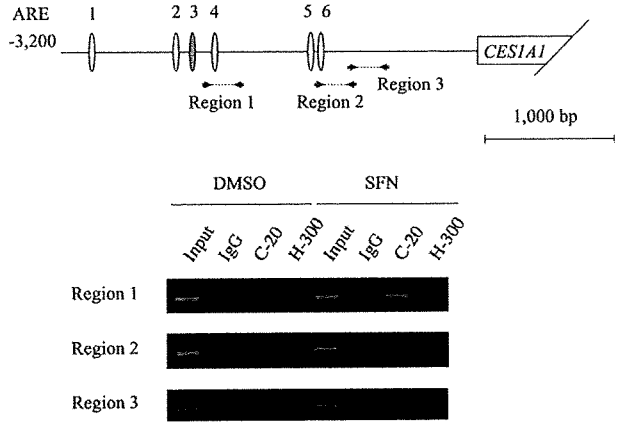

Fig. 6. ChIP assays of Nrf2 binding to the *CES1A1* gene in HepG2 cells. Schematic diagram of the *CES1A1* gene is shown at the top. ChIP assays were performed as described in Section 2. HepG2 cells were treated with 10 μM SFN or DMSO vehicle (0.1%) for 24 h. Rabbit anti-Nrf2 antibodies (C-20 and H-300) and normal rabbit IgG were used for immunoprecipitation of protein–DNA complexes. DNA fragments amplified by PCR were analyzed on 2% agarose gel.

immunoprecipitants of SFN-treated HepG2 cells obtained with anti-Nrf2 antibody (C-20) generated PCR products for region 1 containing functional ARE, but those obtained with anti-Nrf2 antibody (H-300) or normal rabbit IgG did not. Anti-Nrf2 antibody (C-20) recognizes the C-terminal of Nrf2, whereas anti-Nrf2 antibody (H-300) recognizes the N-terminal. This difference in the recognition sites between anti-Nrf2 antibodies (C-20 and H-300) may affect the results in EMSA and the ChIP assays.

Deng et al. [39] and Wu et al. [40] reported that the cholesterol-lowering drug probucol induces HO-1 via oxidative stress. Aburaya et al. [41] reported that Nrf2 is activated by non-steroidal anti-inflammatory drugs (NSAIDs), such as indomethacin, diclofenac, ibuprofen and aspirin. Moreover, isothiocyanates such as SFN and phenethyl isothiocyanate are found broadly distributed among cruciferous vegetables, e.g., cabbage and broccoli. It was reported that the intake of cruciferous vegetables for 2 weeks lowers serum bilirubin concentrations (from 15.73 to 14.02 μmol/L) by up-regulating UGT1A1 activity [42]. In human skin, NQO1 activity is induced up to 1.5-fold by sulforaphane-containing broccoli sprouts [43]. Because CES1A is involved in the metabolism of a number of clinically used drugs and prodrugs, the combined use of drugs or dietary foods that activate Nrf2 might affect the drug response.

In conclusion, we found that Nrf2 transcriptionally activates CES1A1 through binding to the ARE in the 5′-flanking region. This is the first study to demonstrate the molecular mechanism of the inducible regulation of human CES1A1.

Acknowledgement

We acknowledge Mr. Brent Bell for reviewing the manuscript.

References

[1] Song JC, White CM. Clinical pharmacokinetics and selective pharmacodynamics of new angiotensin converting enzyme inhibitors: an update. Clin Pharmacokinet 2002;41:207–24.
[2] Shi D, Yang J, Yang D, LeCluyse EL, Black C, You L, et al. Anti-influenza prodrug oseltamivir is activated by carboxylesterase human carboxylesterase 1, and the activation is inhibited by antiplatelet agent clopidogrel. J Pharmacol Exp Ther 2007;319:1477–84.
[3] Humerickhouse R, Lohrbach K, Li L, Bosron WF, Dolan ME. Characterization of CPT-11 hydrolysis by human liver carboxylesterase isoforms hCE-1 and hCE-2. Cancer Res 2000;60:1189–92.
[4] Pindel EV, Kedishvili NY, Abraham TL, Brzezinski MR, Zhang J, Dean RA, et al. Purification and cloning of a broad substrate specificity human liver carboxylesterase that catalyzes the hydrolysis of cocaine and heroin. J Biol Chem 1997;272:14769–75.
[5] Dolinsky VW, Gilham D, Alam M, Vance DE, Lehner R. Triacylglycerol hydrolase: role in intracellular lipid metabolism. Cell Mol Life Sci 2004;61:1633–51.
[6] Becker A, Böttcher A, Lackner KJ, Fehringer P, Notka F, Aslanidis C, et al. Purification, cloning, and expression of a human enzyme with acyl coenzyme A: cholesterol acyltransferase activity, which is identical to liver carboxylesterase. Arterioscler Thromb 1994;14:1346–55.
[7] Zhao B, Natarajan R, Ghosh S. Human liver cholesteryl ester hydrolase: cloning, molecular characterization, and role in cellular cholesterol homeostasis. Physiol Genomics 2005;23:304–10.
[8] Satoh T, Taylor P, Bosron WF, Sanghani SP, Hosokawa M, La Du BN. Current progress on esterases: from molecular structure to function. Drug Metab Dispos 2002;30:488–93.
[9] Hosokawa M, Furihata T, Yaginuma Y, Yamamoto N, Koyano N, Fujii A, et al. Genomic structure and transcriptional regulation of the rat, mouse, and human carboxylesterase genes. Drug Metab Rev 2007;39:1–15.
[10] Fukami T, Nakajima M, Maruichi T, Takahashi S, McLeod HL, Takamiya M, et al. Structure and characterization of human carboxylesterase 1A1, 1A2, and 1A3 genes. Pharmacogenet Genomics 2008;18:911–20.
[11] Nioi P, McMahon M, Itoh K, Yamamoto M, Hayes JD. Identification of a novel Nrf2-regulated antioxidant response element (ARE) in the mouse NAD(P)H:-quinone oxidoreductase 1 gene: reassessment of the ARE consensus sequence. Biochem J 2003;374:337–48.
[12] Balogun E, Hoque M, Gong P, Killeen E, Green CJ, Foresti R, et al. Curcumin activates the haem oxygenase-1 gene via regulation of Nrf2 and the antioxidant-responsive element. Biochem J 2003;371:887–95.
[13] Yueh MF, Tukey RH. Nrf2-Keap1 signaling pathway regulates human UGT1A1 expression in vitro and in transgenic UGT1 mice. J Biol Chem 2007;282:8749–58.

[14] Moi P, Chan K, Asunis I, Cao A, Kan YW. Isolation of NF-E2-related factor 2 (Nrf2), a NF-E2-like basic leucine zipper transcriptional activator that binds to the tandem NF-E2/AP1 repeat of the β-globin locus control region. Proc Natl Acad Sci USA 1994;91:9926–30.
[15] Motohashi H, O'Connor T, Katsuoka F, Engel JD, Yamamoto M. Integration and diversity of the regulatory network composed of Maf and CNC families of transcription factors. Gene 2002;294:1–12.
[16] Nerland DE. The antioxidant/electrophile response element motif. Drug Metab Rev 2007;39:235–48.
[17] Itoh K, Chiba T, Takahashi S, Ishii T, Igarashi K, Katoh Y, et al. An Nrf2/small Maf heterodimer mediates the induction of phase II detoxifying enzyme genes through antioxidant response elements. Biochem Biophys Res Commun 1997;236:313–22.
[18] Li W, Kong AN. Molecular mechanisms of Nrf2-mediated antioxidant response. Mol Carcinog 2009;48:91–104.
[19] Hosokawa M, Furihata T, Yaginuma Y, Yamamoto N, Watanabe N, Tsukada E, et al. Structural organization and characterization of the regulatory element of the human carboxylesterase (CES1A1 and CES1A2) genes. Drug Metab Pharmacokinet 2008;23:73–84.
[20] Nishimura M, Imai T, Morioka Y, Kuribayashi S, Kamataki T, Naito S. Effects of NO-1886 (Ibrolipim), a lipoprotein lipase-promoting agent, on gene induction of cytochrome P450s, carboxylesterases, and sulfotransferases in primary cultures of human hepatocytes. Drug Metab Pharmacokinet 2004;19:422–9.
[21] Takakusa H, Masumoto H, Mitsuru A, Okazaki O, Sudo K. Markers of electrophilic stress caused by chemically reactive metabolites in human hepatocytes. Drug Metab Dispos 2008;36:816–23.
[22] Tsuchiya Y, Nakajima M, Kyo S, Kanaya T, Inoue M, Yokoi T. Human CYP1B1 is regulated by estradiol via estrogen receptor. Cancer Res 2004;64:3119–25.
[23] Sanghani SP, Quinney SK, Fredenburg TB, Sun Z, Davis WI, Murry DJ, et al. Carboxylesterases expressed in human colon tumor tissue and their role in CPT-11 hydrolysis. Clin Cancer Res 2003;9:4983–91.
[24] Nakamura A, Nakajima M, Higashi E, Yamanaka H, Yokoi T. Genetic polymorphisms in the 5′-flanking region of human UDP-glucuronosyltransferase 2B7 affect the Nrf2-dependent transcriptional regulation. Pharmacogenet Genomics 2008;18:709–20.
[25] Laemmli UK. Cleavage of structural proteins during the assembly of the head of bacteriophage T4. Nature 1970;227:680–5.
[26] Bradford MM. A rapid and sensitive method for the quantitation of microgram quantities of protein utilizing the principle of protein-dye binding. Anal Biochem 1976;72:248–54.
[27] Takahashi S, Katoh M, Saitoh T, Nakajima M, Yokoi T. Allosteric kinetics of human carboxylesterase1: species difference and interindividual variability. J Pharm Sci 2008;97:5434–45.
[28] Horton RM, Cai ZL, Ho SN, Pease LR. Gene splicing by overlap extension: tailor-made genes using the polymerase chain reaction. Biotechniques 1990;8:528–35.
[29] Zhang DD. Mechanistic studies of the Nrf2-Keap1 signaling pathway. Drug Metab Rev 2006;38:769–89.
[30] Gharavi N, El-Kadi AO. tert-Butylhydroquinone is a novel aryl hydrocarbon receptor ligand. Drug Metab Dispos 2005;33:365–72.
[31] Anwar-Mohamed A, El-Kadi AO. Sulforaphane induces CYP1A1 mRNA, protein, and catalytic activity levels via an AhR-dependent pathway in murine hepatoma Hepa 1c1c7 and human HepG2 cells. Cancer Lett 2009;275:93–101.
[32] Marchand A, Barouki R, Garlatti M. Regulation of NAD(P)H:quinone oxidoreductase 1 gene expression by CYP1A1 activity. Mol Pharmacol 2004;65:1029–37.
[33] Elbekai RH, El-Kadi AO. Transcriptional activation and posttranscriptional modification of Cyp1a1 by arsenite, cadmium, and chromium. Toxicol Lett 2007;172:106–19.
[34] Sugatani J, Mizushima K, Osabe M, Yamakawa K, Kakizaki S, Takagi H, et al. Transcriptional regulation of human UGT1A1 gene expression through distal and proximal promoter motifs: implication of defects in the UGT1A1 gene promoter. Naunyn Schmiedebergs Arch Pharmacol 2008;377:597–605.
[35] Thimmulappa RK, Mai KH, Srisuma S, Kensler TW, Yamamoto M, Biswal S. Identification of Nrf2-regulated genes induced by the chemopreventive agent sulforaphane by oligonucleotide microarray. Cancer Res 2002;62:5196–203.
[36] Cho HY, Reddy SP, Yamamoto M, Kleeberger SR. The transcription factor NRF2 protects against pulmonary fibrosis. FASEB J 2004;18:1258–60.
[37] Forkert PG, Lee RP, Reid K. Involvement of CYP2E1 and carboxylesterase enzymes in vinyl carbamate metabolism in human lung microsomes. Drug Metab Dispos 2001;29:258–63.
[38] Vidali M, Tripodi MF, Ivaldi A, Zampino R, Occhino G, Restivo L, et al. Interplay between oxidative stress and hepatic steatosis in the progression of chronic hepatitis C. J Hepatol 2008;48:399–406.
[39] Deng YM, Wu BJ, Witting PK, Stocker R. Probucol protects against smooth muscle cell proliferation by upregulating heme oxygenase-1. Circulation 2004;110:1855–60.
[40] Wu BJ, Kathir K, Witting PK, Beck K, Choy K, Li C, et al. Antioxidants protect from atherosclerosis by a heme oxygenase-1 pathway that is independent of free radical scavenging. J Exp Med 2006;203:1117–27.
[41] Aburaya M, Tanaka K, Hoshino T, Tsutsumi S, Suzuki K, Makise M, et al. Heme oxygenase-1 protects gastric mucosal cells against non-steroidal anti-inflammatory drugs. J Biol Chem 2006;281:33422–32.
[42] Navarro SL, Peterson S, Chen C, Makar KW, Schwarz Y, King IB, et al. Cruciferous vegetable feeding alters UGT1A1 activity: diet- and genotype-dependent changes in serum bilirubin in a controlled feeding trial. Cancer Prev Res (Phila Pa) 2009;2:345–52.
[43] Dinkova-Kostova AT, Fahey JW, Wade KL, Jenkins SN, Shapiro TA, Fuchs EJ, et al. Induction of the phase 2 response in mouse and human skin by sulforaphane-containing broccoli sprout extracts. Cancer Epidemiol Biomarkers Prev 2007;16:847–51.

Interactions Between Human UDP-Glucuronosyltransferase (UGT) 2B7 and UGT1A Enzymes

RYOICHI FUJIWARA,[1] MIKI NAKAJIMA,[1] SHINGO ODA,[1] HIROYUKI YAMANAKA,[1] SHIN-ICHI IKUSHIRO,[2] TOSHIYUKI SAKAKI,[2] TSUYOSHI YOKOI[1]

[1]Drug Metabolism and Toxicology, Faculty of Pharmaceutical Sciences, Kanazawa University, Kakuma-machi, Kanazawa 920-1192, Japan

[2]Food Science and Technology, Biotechnology Research Center, Faculty of Engineering, Toyama Prefectural University, Toyama, Japan

Received 16 February 2009; revised 23 April 2009; accepted 28 April 2009

Published online 27 May 2009 in Wiley InterScience (www.interscience.wiley.com). DOI 10.1002/jps.21830

ABSTRACT: Glucuronidation catalyzed by UDP-glucuronosyltransferase (UGT) enzymes is an important pathway in the metabolism of drugs as well as environmental chemicals. In this study, protein–protein interactions between human UGT2B7 and UGT1As and their effects on the enzymatic activities were investigated using double expression systems in HEK293 cells (UGT2B7/UGT1A1, UGT2B7/UGT1A4, UGT2B7/UGT1A6, and UGT2B7/UGT1A9). Native-PAGE analysis clearly revealed that UGT2B7 forms homo-oligomers. Furthermore, hetero-oligomers of UGT2B7 with UGT1As were observed by native-PAGE analysis. Immunoprecipitation assay revealed associations of UGT2B7 with UGT1A1, UGT1A4, UGT1A6, and UGT1A9. The thermal stability of UGT2B7 was significantly increased by the coexpressed UGT1A1, UGT1A4, UGT1A6, and UGT1A9, indicating an interaction between UGT2B7 and the UGT1As. To examine the effects of the protein–protein interactions on the enzymatic activities, kinetic analyses were performed. Coexpression of the UGT1As significantly decreased K_m and increased V_{max} of zidovudine *O*-glucuronidation by UGT2B7. Coexpression of UGT2B7 also affected the kinetics of estradiol 3-*O*-glucuronidation by UGT1A1, imipramine *N*-glucuronidation by UGT1A4, serotonin *O*-glucuronidation by UGT1A6, and propofol *O*-glucuronidation by UGT1A9. In conclusion, it was clearly demonstrated that human UGT2B7 interacts with UGT1A enzymes, affecting their kinetics. That such interactions might occur in human liver microsomes underscores the complexities in glucuronidations in human liver. © 2009 Wiley-Liss, Inc. and the American Pharmacists Association J Pharm Sci 99:442–454, 2010

Keywords: hepatic metabolism; enzyme kinetics; phase II enzymes; glucuronosyltransferases (UGT); metabolic clearance

INTRODUCTION

UDP-Glucuronosyltransferases (UGTs) catalyze the conjugation of endogenous and exogenous compounds with UDP-glucuronic acid (UDPGA).[1] Human UGTs are classified into three subfamilies, UGT1A, UGT2A, and UGT2B, based on evolutionary divergence.[2] The human *UGT1A* gene cluster located on chromosome 2q37 contains multiple unique first exons for each UGT1A, with exons 2–5 in common,[3] encoding nine kinds of functional UGT1As. The *UGT2A* and *UGT2B* genes are located on chromosome 4q13, encoding three and seven functional proteins, respectively. UGT2A1 and UGT2A2 are formed by differential splicing of variable first exons and the common

Abbreviations: UGT, UDP-glucuronosyltransferase; UDPGA, UDP-glucuronic acid; HPLC, high performance liquid chromatography.

Correspondence to: Tsuyoshi Yokoi (Telephone: 81-76-234-4407; Fax: 81-76-234-4407;
E-mail: tyokoi@kenroku.kanazawa-u.ac.jp)

Journal of Pharmaceutical Sciences, Vol. 99, 442–454 (2010)

exons 2–6, likely the *UGT1A* gene. However, UGT2A3 and each UGT2B are encoded by individual genes. Human UGTs are expressed in a tissue-specific manner.[4] Previous studies using reverse transcription-polymerase chain reaction (PCR) revealed that UGT1A1, UGT1A3, UGT1A4, UGT1A6, UGT1A9, UGT2B4, UGT2B7, UGT2B10, UGT2B11, UGT2B15, and UGT2B17 are expressed in human liver.[4–6]

Mammalian UGTs are located on the endoplasmic reticulum membrane and most of their mass is in the luminal side. That UGTs form homo- or hetero-oligomers was revealed by a variety of techniques including gel permeation chromatography,[7] radiation inactivation analysis,[8,9] a cross-linking study,[10] SDS–PAGE,[11] two-hybrid analysis,[12] a heterologous expression study,[13,14] immobilized metal-chelating chromatography,[15] and fluorescence resonance energy transfer method.[16] Using the heterologous expression technique, we demonstrated that human UGT1A1, UGT1A4, UGT1A6, and UGT1A9 interact with each other via heterodimerization. The heterodimerization of these UGT1A enzymes caused diverse changes of enzyme activities depending on the UGT isoforms and substrates.[17–19] In the present study, we expanded our examination of UGT2B7, because UGT2B7 is the most important isoform for the metabolism of clinically used drugs such as morphine, zidovudine, and valproic acid[20] and is expressed in various tissues including liver, intestine, and kidney. Kurkela et al.[21] has reported that coexpressed UGT1A6 decreased the activity of UGT2B7, but their interaction was not directly proven. Furthermore, there is no information on the interactions between UGT2B7 and the other human UGT1As. In this study, to understand the interactions between UGT2B7 and UGT1A enzymes, we established double expression systems of UGT2B7/UGT1A1, UGT2B7/UGT1A4, UGT2B7/UGT1A6, and UGT2B7/UGT1A9 in HEK293 cells. By native-PAGE analysis, immunoprecipitation assay, and thermal stability assay, we evaluated the significance of the interactions between UGT2B7 and UGT1A enzymes. Finally, the effects of the interactions on their enzyme activities were assessed.

MATERIALS AND METHODS

Chemicals and Reagents

UDPGA, alamethicin, estradiol, and estradiol 3-glucuronide were purchased from Sigma–Aldrich (St. Louis, MO). Zidovudine, imipramine, serotonin, propofol, and G418 were from Wako Pure Chemicals Industries (Osaka, Japan). Zidovudine *O*-glucuronide was obtained from Toronto Research Chemicals (Toronto, Canada). Rabbit anti-human UGT1A polyclonal antibody, rabbit anti-human UGT1A1 polyclonal antibody, rabbit anti-human UGT2B7 polyclonal antibody, and human liver microsomes from 11 individuals were obtained from BD Gentest (Woburn, MA). Rabbit anti-human UGT2B polyclonal antibody (H-300) and goat anti-human UGT2B polyclonal antibody (F-17) were purchased from Santa Cruz Biotechnology (San Diego, CA). Mouse anti-KDEL monoclonal antibody was obtained from Stressgen Biotechnologies (San Diego, CA). Perfect NT Gel M was purchased from DRC (Tokyo, Japan). Primers were commercially synthesized at Hokkaido System Sciences (Sapporo, Japan). All other chemicals and solvents were of analytical grade or the highest grade commercially available.

Stable Single and Double UGT Expression Systems in HEK293 Cells

Expression vectors for human UGT1A1, UGT1A4, UGT1A6, and UGT1A9 were previously constructed.[18] Human UGT2B7 (accession number NM_001074) cDNA was prepared by a reverse transcription-PCR technique from human liver total RNA with sense and antisense oligonucleotide primers (5′-ATT GCA CCA GGA TGT CTG-3′ and 5′-CTT GCA TCA CAA TCT TTC TTG CTG-3′). The PCR products were subcloned into pTARGET Mammalian Expression Vector (Promega, Madison, WI) and the DNA sequences of the inserts were determined using a Thermo Sequenase Cy5.5 Dye Terminator Cycle Sequencing kit (GE Healthcare Bio-Science, Piscataway, NJ) with a Long-Read Tower DNA sequencer (GE Healthcare Bio-Science). HEK293 cells (American Type Culture Collection, Manassas, VA) were grown in Dulbecco's modified Eagle's medium containing 4.5 g/L glucose, 10 mM HEPES, and 10% fetal bovine serum with 5% CO_2 at 37°C. Two micrograms of the UGT expression vector were transfected into HEK293 cells in 6-well plates with Lipofectamine (Invitrogen, Carlsbad, CA). For the double expression systems, the expression vector for UGT2B7 was simultaneously transfected into the cells with each UGT1A expression vector (UGT1A1, UGT1A4, UGT1A6, or UGT1A9) at the ratio of 1:1. Stable transfectants were

selected in medium containing 800 μg/mL G418 and several clones were isolated.

SDS–PAGE or Native-PAGE and Immunoblot Analysis

To determine the expression levels of UGT2B7 and UGT1As in the constructed recombinant systems, SDS–PAGE and immunoblot analysis were performed using anti-UGT2B and anti-UGT1A antibodies and an Odyssey infrared imaging system (Li-COR Biosciences, Lincoln, NE). Since the titer of the rabbit anti-UGT2B antibody was higher than that of the rabbit anti-UGT2B7 antibody, the rabbit anti-UGT2B antibody was used. Although it was confirmed that UGT enzymes are expressed in microsomes fraction, total cell homogenates prepared as described previously[18] were used for convenience in this study. The total cell homogenates (10 μg of protein) were subjected to 10% SDS–PAGE and transferred to a PVDF membrane Immobilon-P (Millipore, Bedford, MA). The membrane was washed with phosphate buffered saline (PBS) two times and blocked with Odyssey Blocking Buffer (Li-COR Biosciences) for 1 h. The membrane was probed with the primary antibody diluted (1:500) with Odyssey Blocking Buffer containing 0.1% Tween-20 for 1 h. The membrane was washed with PBST (PBS containing 0.1% Tween-20) four times and incubated with IRDye680-labeled goat anti-rabbit secondary antibody diluted (1:5000) with PBST for 1 h. The densities of the bands were determined using the Odyssey infrared imaging system. Although the expression levels of UGT2B7 and UGT1As cannot be simply compared because the primary antibodies are different, the relative expression levels of UGT2B7 and UGT1A1 were defined based on standard curves using their single expression systems (1 U/1 mg of cell homogenates) for convenience.

To determine the expression levels of UGT2B7 and UGT1A1 proteins in human liver microsomes, SDS–PAGE and immunoblot analysis were performed using anti-UGT2B7 and anti-UGT1A1 antibodies. For the quantification, the UGT2B7 and UGT1A1 single expression systems were used to make the standard curves as described above.

Native-PAGE analysis was performed to detect monomer and oligomer formations of UGTs as described previously[17] with slight modifications. Ten to 100 μg of total cell homogenates were lysed in solubilizing buffer (0.5% NP-40, 0.25% sodium deoxycholate, 50 mM Tris–HCl (pH 7.5), 150 mM NaCl, and 1 mM EDTA) on ice for 2 h. After centrifugation at 13,000*g* for 30 min, 1 μL of 60% glycerol containing 0.2% bromophenol blue was added to a 20-μL portion of the supernatant. The samples were applied to Perfect NT Gel M (5–20% gradient) and the electrophoresis was carried out at 10 mA for 5 h at 4°C in Tris–glycine electrophoresis buffer (25 mM Tris–base, 192 mM glycine, and 0.1% SDS). The separated proteins were transferred to a PVDF membrane and probed with the anti-UGT2B and anti-UGT1A antibodies as described above.

Immunoprecipitation

Rabbit anti-human UGT1A antibody (BD Gentest) or rabbit anti-human UGT1AC antibody[22] against common carboxyl-terminal region of UGT1A was cross-linked with protein-Sepharose CL-4B (GE Healthcare Bio-Sciences) as described previously.[18] The beads were resuspended in solubilizing buffer (0.5% NP-40, 0.25% deoxycholate, 50 mM Tris–HCl (pH 7.5), 150 mM NaCl, 1 mM EDTA). Cell homogenates (500 μg) were solubilized with the solubilizing buffer in a final concentration of 1.0 mg/mL at 4°C for 2 h. After centrifugation at 13,000*g* for 30 min at 4°C, the supernatants were incubated with the beads at 4°C for 14 h. The beads were washed three times with the solubilizing buffer. The bound proteins were eluted with 2 M guanidine hydrochloride for 6 h at room temperature. The eluates were subjected to SDS–PAGE followed by immunoblot analysis with anti-UGT1A, rabbit or goat anti-UGT2B, and anti-KDEL antibodies.

Glucuronide Formation

Zidovudine *O*-glucuronide formation was determined according to a method by Court et al.[23] with slight modifications. A typical incubation mixture (200 μL total volume) contained 50 mM phosphate buffer (pH 7.4), 5 mM $MgCl_2$, 5 mM UDPGA, 0.2 mg/mL total cell homogenates, alamethicin (50 μg/mg of protein), and 0.25–1.2 mM zidovudine. The reaction was initiated by the addition of UDPGA following a 2 min preincubation at 37°C. The incubation mixture was incubated at 37°C for 60 min, since it was confirmed that the zidovudine *O*-glucuronide formation was linear over 90 min. After the incubation, the reaction was terminated by the addition of 10 μL of 30% perchloric acid.

The reaction mixture was centrifuged at 7,000*g* for 10 min, and 60 μL of the supernatant was subjected to HPLC. The analytical column was an Inertsil ODS-3 (4.6 mm × 250 mm; 5 μm) (GL Sciences, Tokyo, Japan). The mobile phase was 10% acetonitrile/10 mM potassium phosphate buffer (pH 2.3) and the flow rate was 1.0 mL/min. The column eluate was monitored at 267 nm. The retention times of zidovudine *O*-glucuronide and zidovudine were 10.4 and 15.0 min, respectively. The quantification of zidovudine *O*-glucuronide was made by comparing the HPLC peak height to that of the authentic standard.

For the study of thermal stability, reaction mixtures containing the cell homogenate were treated at 47°C for 15 min in the presence of UDPGA. Then, zidovudine was added to the mixture at a final concentration of 250 μM and the mixture was incubated at 37°C for 60 min to determine the residual enzyme activity.

Estradiol 3-*O*-glucuronide formation, imipramine *N*-glucuronide formation, serotonin *O*-glucuronide formation, and propofol *O*-glucuronide formation were determined as described previously.[18]

Kinetic parameters were estimated from the fitted curve using a computer program (KaleidaGraph, Synergy Software, Reading, PA) designed for nonlinear regression analysis. The following equations were used:

Michaelis–Menten equation

$$V = \frac{V_{max}[S]}{K_m + [S]}$$

Hill equation

$$V = \frac{V_{max}[S]^n}{S_{50}^n + [S]^n}$$

Substrate inhibition equation

$$V = \frac{V_{max}[S]}{K_m + [S] + [S]^2/K_i}$$

where V is the velocity of the reaction, S the substrate concentration, K_m the Michaelis–Menten constant, V_{max} the maximum velocity, S_{50} the substrate concentration showing the half V_{max}, n the Hill coefficient, and K_i the substrate inhibition constant. For the Michaelis–Menten kinetics and the substrate inhibition kinetics, the intrinsic clearance (CL_{int}) was calculated as the V_{max}/K_m. For sigmoidal kinetic data, the maximum clearance (CL_{max}), which has been proposed as an appropriate parameter instead of the intrinsic clearance,[24,25] was calculated by the following equation:

$$CL_{max} = \frac{V_{max}}{S_{50}} \frac{(n-1)}{n(n-1)^{1/n}}$$

Statistical Analyses

Data are expressed as mean ± SD of three independent determinations. The statistical significance of the kinetic parameters was determined by analysis of variance (ANOVA) followed by Dunnett's test. A value of $P < 0.05$ was considered statistically significant.

RESULTS

Establishment of Single and Double Expression Systems of UGT2B7 and UGT1As in HEK293 Cells

To investigate whether human UGT2B7 interacts with UGT1A enzymes, stable single expression systems (UGT2B7, UGT1A1, UGT1A4, UGT1A6, and UGT1A9) and double expression systems (UGT2B7/UGT1A1, UGT2B7/UGT1A4, UGT2B7/UGT1A6, and UGT2B7/UGT1A9) in HEK293 cells were constructed. The expression levels of UGT protein were determined by immunoblot analysis (Fig. 1A). The expression levels of UGT2B7 and UGT1A1 in the single expression system were defined as 1.00 U/mg. Based on the expression level of UGT1A1 in the single expression system, the UGT1A4, UGT1A6, and UGT1A9 levels in single expression systems were estimated as 0.18, 0.13, and 0.35 U/mg protein, respectively. In two clones of the double expression system for UGT2B7/UGT1A1, the expression levels of UGT2B7 (0.10 and 0.14 U/mg) and UGT1A1 (0.51 and 0.12 U/mg) resulted in a 2B7/1A ratio 0.2 and 1.2. In two clones of the double expression system for UGT2B7/UGT1A4, the expression levels of UGT2B7 (0.12 and 0.27 U/mg) and UGT1A4 (0.79 and 0.24 U/mg) resulted in a 2B7/1A ratio 0.2 and 1.1. In two clones of the double expression system for UGT2B7/UGT1A6, the expression levels of UGT2B7 (0.22 and 0.12 U/mg) and UGT1A6 (0.57 and 0.09 U/mg) resulted in a 2B7/1A ratio 0.4 and 1.3. In two clones of the double expression system for UGT2B7/UGT1A9, the expression levels of UGT2B7 (0.10 and 0.19 U/mg) and UGT1A9 (0.22 and 0.07 U/mg) resulted in a 2B7/1A ratio 0.5 and 2.7.

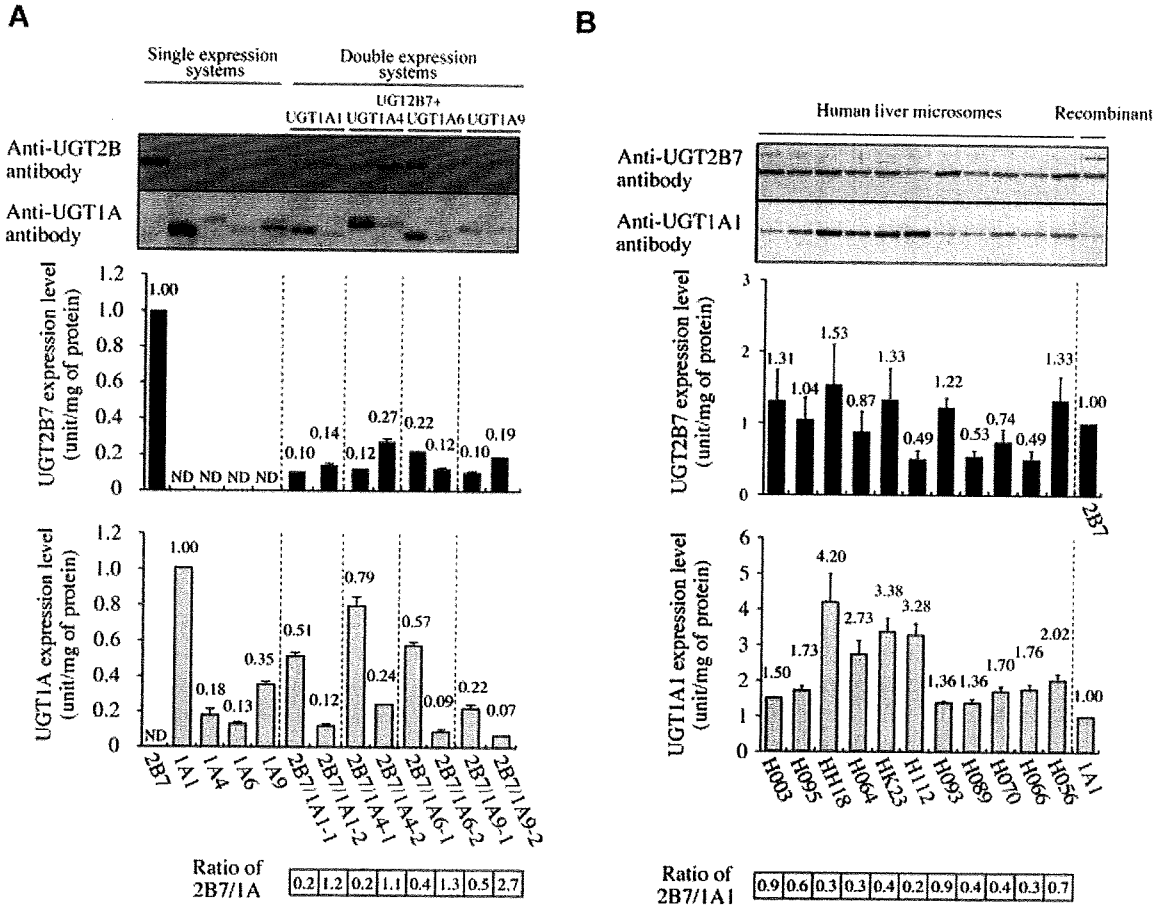

Figure 1. Immunoblot analysis of human UGT2B7 and UGT1As in the single and double expression systems as well as human liver microsomes. The total cell homogenates from the HEK293 expression systems (10 μg protein) were subjected to 10% SDS–PAGE and the membranes were probed with the anti-human UGT2B and anti-human UGT1A antibodies (A). For the analysis of UGT2B7 and UGT1A1 in human liver microsomes, 5- and 2-μg protein of human liver microsomes, respectively, were applied and the membranes were probed with anti-human UGT2B7 and anti-human UGT1A1 antibodies (B). The rightmost lane in the membranes shows the UGT2B7 single expression system (5 μg protein) and the UGT1A1 single expression system (2 μg protein). The expression levels of UGT2B7 and UGT1As were defined based on standard curves using the UGT2B7 and UGT1A1 single expression systems (1 U/1 mg of cell homogenates). Columns are the mean ± SD of three independent determinations.

Expression Levels of UGT1A1 and UGT2B7 Proteins in Human Liver Microsomes

To investigate how similar the UGT2B7/UGT1A ratios in our expression systems were to those in human liver microsomes, we determined the expression levels of UGT2B7 and UGT1A1 protein in human liver microsomes by immunoblot analyses. Since human liver microsomes express multiple UGT isoforms, the specific antibodies against UGT2B7 or UGT1A1 were used. The expression levels were quantified using standard curves of the UGT2B7 and UGT1A1 single expression systems in HEK293 cells. The expression level of UGT2B7 and UGT1A1 proteins in 11 individual human liver microsomes ranged from 0.49 to 1.53 and 1.36 to 4.20 U/mg of protein, respectively (Fig. 1B). The UGT2B7/UGT1A1 ratios ranged from 0.2 to 0.9. These results suggest that the ratios of UGT2B7/UGT1A in our expression systems were similar to the ratios of UGT2B7/UGT1A1 in human liver microsomes.

DOI 10.1002/jps

Native-PAGE Analysis of Single and Double Expression Systems

Native-PAGE analysis was performed to investigate the oligomerizations of human UGT2B7 and UGT1As. First, we confirmed that UGT enzymes were efficiently solubilized with the solubilizing buffer (data not shown). When the total cell homogenate of the single expression system of UGT2B7 was separated, three bands were observed at about 50, 100, and 130 kDa (Fig. 2, arrows 1–3, respectively). These three bands were also observed in the double expression systems of UGT2B7 and UGT1As, but not in Mock cells and the single expression systems of UGT1As. The lower (arrow 1) and middle (arrow 2) bands would correspond to monomers and homodimers, respectively. The upper band (arrow 3) might be an oligomeric form of UGT2B7 that is greater than the dimer. In our previous study,[17] when the double expression system of UGT1A1/UGT1A4 was applied for the native-PAGE analysis, a unique band corresponding to a heterodimer was observed. Interestingly, several bands were detected at around 150–250 kDa in the double expression of UGT2B7 and UGT1As, but not in the single expression system of UGT2B7. Therefore, these unique bands might represent hetero-oligomers of UGT2B7 and UGT1As. To further investigate the hetero-oligomerizations between UGT2B7 and UGT1As, coimmunoprecipitation and thermal stability assay were performed.

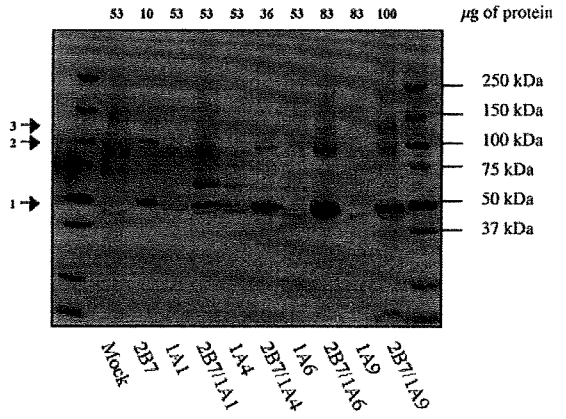

Figure 2. Native-PAGE analyses of UGT2B7 and UGT1As in the single and double expression systems. As the double expression systems, the 2B7/1A1-2, 2B7/1A4-2, 2B7/1A6-2, and 2B7/1A9-2 clones were used. Solubilized total cell homogenates were subjected to gradient gel (5–20%). After electrophoresis at 4°C, the proteins were transferred to a PVDF membrane and immunoblotted with rabbit anti-human UGT2B antibody. Arrows 1–3 represent the bands corresponding to monomer, homodimer, and homo-oligomers of UGT2B7, respectively.

Coimmunoprecipitation of UGT2B7 with Anti-Human UGT1A Antibody

To investigate the association between UGT2B7 and the UGT1A enzymes, immunoprecipitation analysis was carried out using anti-human UGT1A antibody (Fig. 3A). Using the single expression systems, it was confirmed that the anti-human UGT1A antibody specifically immunoprecipitated the UGT1As. When the double expression systems were used, UGT2B7 protein was coimmunoprecipitated by the anti-human UGT1A antibody, although the band density of the UGT2B7 from the double expression system for UGT2B7/1A1 was weaker than those of the other double expression systems. Glucose-regulated protein 94 (GRP94) and GRP78 that are expressed in endoplasmic reticulum were not detected in the immunoprecipitants, indicating the specific interaction between UGT2B7 and the UGT1As. When the anti-human UGT1AC antibody was used for immunoprecipitation, UGT2B7 protein was coimmunoprecipitated from the double expression systems (Fig. 3B). Especially, the band density from the double expression systems for UGT2B7/1A4 and UGT2B7/UGT1A9 was substantial. It was confirmed that UGT1As were immunoprecipitated by the anti-human UGT1AC antibody, and that GRP94 and GRP78 were not detected in the immunoprecipitants. The results suggest that UGT2B7 specifically interacts with the UGT1A enzymes.

Effects of Coexpression of UGT1A on Thermal Instability of UGT2B7

Thermal instability is a useful tool for analyzing protein–protein interactions.[18] As a specific activity for UGT2B7, zidovudine *O*-glucuronidation was measured, since we confirmed that UGT1A1, UGT1A4, UGT1A6, and UGT1A9 could not catalyze this reaction (data not shown). The enzymatic activities in the single and double expression systems were normalized with the UGT2B7 protein levels by immunoblot analysis. Zidovudine *O*-glucuronide formation by the UGT2B7 single expression system was decreased to 5% of control by heat treatment at 47°C for 15 min (Fig. 4), indicating that UGT2B7 is thermally

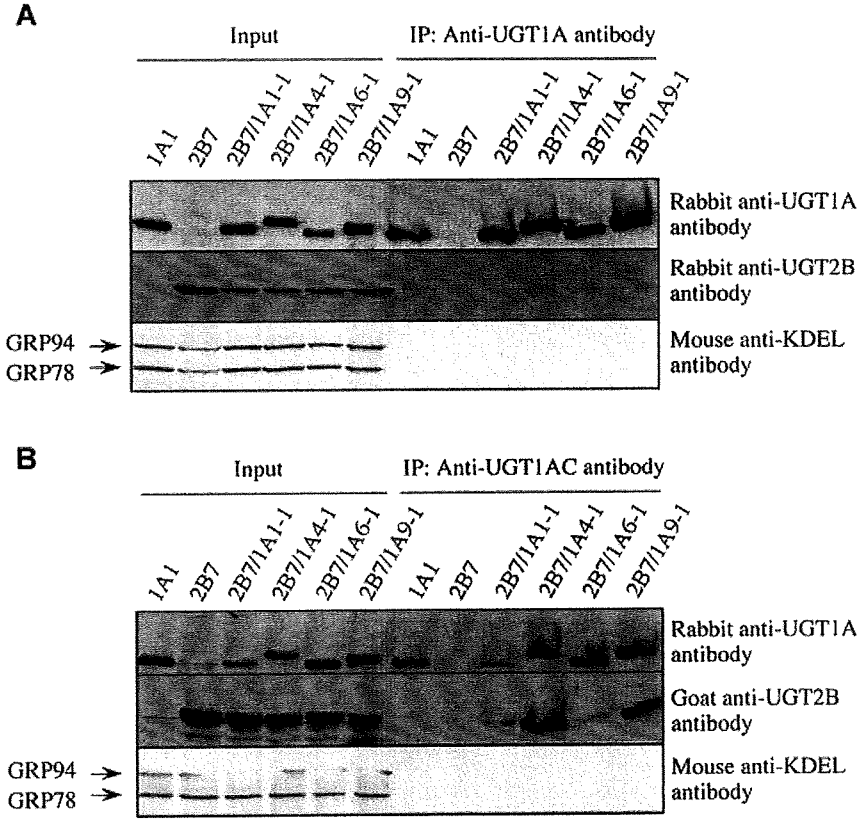

Figure 3. Coimmunoprecipitation of UGT2B7 by anti-human UGT1A antibody using the double expression systems of UGT2B7/UGT1As. Rabbit anti-human UGT1A antibody from BD Gentest (A) or rabbit anti-human UGT1AC antibody prepared by Ikushiro et al.[22] (B) were used for immunoprecipitation. The input proteins and coimmunoprecipitants were subjected to SDS–PAGE followed by immunoblot analysis using anti-human UGT1A, anti-human UGT2B. Anti-KDEL antibodies detected GRP94 and GRP78 only in the input proteins.

instable. UGT2B7 in the double expression systems of UGT2B7/UGT1As showed tolerability to the heat treatment. The results suggest that UGT2B7 interacted with UGT1A1, UGT1A4, UGT1A6, and UGT1A9 in the double expression systems.

Kinetic Analyses of Zidovudine, Estradiol, Imipramine, Serotonin, and Propofol Glucuronide Formations

To investigate the effects of the coexpression of UGT1A enzymes on the enzymatic activity of UGT2B7, kinetic analysis of zidovudine *O*-glucuronide formation was carried out using the single and double expression systems. It was confirmed that any UGT1A enzymes did not show a detectable zidovudine *O*-glucuronide formation (data not shown). The zidovudine *O*-glucuronide formation by the single expression system of UGT2B7 in HEK293 cells fitted to the Michaelis–Menten kinetics (Fig. 5A) with $K_m = 282 \pm 16\ \mu M$, $V_{max} = 449 \pm 16$ pmol/min/U, and $CL_{int} = 1.6 \pm 0.1\ \mu L/min/U$ (Tab. 1). The kinetic parameters were reproducible in another clone of the UGT2B7 single expression system (data not shown). By the coexpression of UGT1A1, the V_{max} and CL_{int} values were significantly increased (Fig. 5A and Tab. 1). By the coexpression of UGT1A4, the K_m value was significantly decreased and the V_{max} and CL_{int} values were significantly increased compared with those values in the UGT2B7 single expression system (Fig. 5B and Tab. 1). A significant decrease of K_m and increases of the V_{max} and CL_{int} values were also observed in the

DOI 10.1002/jps

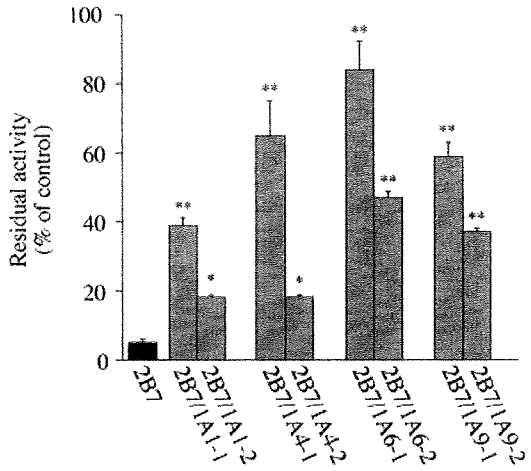

Figure 4. Effect of heat treatment on the enzymatic activities of UGT2B7 in the single and double expression systems. After the preincubation of the total cell homogenates at 47°C for 15 min in the presence of UDPGA, zidovudine *O*-glucuronide formation was measured with 250 μM of substrate. Each column shows the residual activity after the heat treatment. Data are the mean ± SD of three independent determinations. $^{*}P < 0.05$ and $^{**}P < 0.01$ compared with the UGT2B7 single expression system.

double expression systems with UGT1A6 and UGT1A9 (Fig. 5C and D and Tab. 1).

The effects of the coexpression of UGT2B7 on the enzymatic activities of UGT1A1, UGT1A4, UGT1A6, and UGT1A9 were investigated. It was confirmed that the estradiol 3-*O*-glucuronide, imipramine *N*-glucuronide, serotonin *O*-glucuronide, and propofol *O*-glucuronide formations were specifically catalyzed by UGT1A1, UGT1A4, UGT1A6, and UGT1A9, respectively (data not shown). The estradiol 3-*O*-glucuronide formation by the single expression system of UGT1A1 in HEK293 cells followed the Hill equation (Fig. 5E), yielding $S_{50} = 17.5 \pm 3.3$ μM, $V_{max} = 0.8 \pm 0.0$ nmol/min/U, Hill coefficient (n) = 1.4 ± 0.2, and $CL_{max} = 27.0 \pm 2.8$ μL/min/U (Tab. 2). These kinetic parameters were consistent with those of our previous study.[18] By the coexpression of UGT2B7, the S_{50} was significantly decreased and the n value and CL_{max} values were significantly increased (Tab. 2). The imipramine *N*-glucuronide formation by the single expression system of UGT1A4 in HEK293 cells showed substrate inhibition at substrate concentrations >1.5 mM (Fig. 5F). When the kinetics were analyzed by fitting to the Michaelis–Menten kinetics with substrate concentrations up to 1.0 mM, the K_m, V_{max}, and CL_{int} values were 0.6 ± 0.03 mM, 1.4 ± 0.1 nmol/min/U, and 2.3 ± 0.1 μL/min/U, respectively (Tab. 2). By the coexpression of UGT2B7, the K_m and V_{max} values were significantly increased. The serotonin *O*-glucuronide formation by the single expression system of UGT1A6 fitted to the Michaelis–Menten kinetics (Fig. 5G) with $K_m = 7.6 \pm 2.0$ mM, $V_{max} = 2.7 \pm 0.7$ nmol/min/U, and $CL_{int} = 0.4 \pm 0.1$ μL/min/U (Tab. 2). By the coexpression of UGT2B7, the V_{max} and CL_{int} values were increased. The propofol *O*-glucuronide formation by the single expression system of UGT1A9 fitted to the substrate inhibition kinetics (Fig. 5H) with $K_m = 67.7 \pm 5.2$ μM, $V_{max} = 43.7 \pm 3.7$ nmol/min/U, $K_i = 1.0 \pm 0.1$ mM, and $CL_{int} = 0.7 \pm 0.0$ μL/min/U (Tab. 2). The V_{max} and CL_{int} values in the clone 2B7/1A9-1 were significantly increased. These results suggest that UGT2B7 affected the UGT1A1, UGT1A4, UGT1A6, and UGT1A9 activity, and *vice versa*. It was confirmed that mixing of each single expression system did not influence the kinetics of the enzymatic activities (data not shown). Taken together, it is suggested that the coexpressed UGT isoforms functionally interacted with each other in the double expression systems.

DISCUSSION

Accumulating evidence has revealed that UGTs form oligomers.[26] Our previous studies demonstrated that human UGT1A enzymes interact each other via heterodimerization, resulting in changes of the enzymatic properties.[17–19] We expanded out study to investigate whether UGT2B7, one of the major UGT isoforms expressed in human liver, interacts with UGT1As, and to determine the effects of the interaction on the enzymatic activities.

The homo-oligomerizations of human UGT1A enzymes has been demonstrated,[15,16] but it has never been determined whether human UGT2B7 forms homo-oligomers. Previously, we reported that native-PAGE analysis is a useful technique to detect oligomers[17] and we could show the homo-dimerization of UGT1A1, UGT1A4, and UGT1A6. In the present study, the native-PAGE analysis clearly demonstrated the homo-oligomerizations of UGT2B7 (Fig. 2). The results suggested the possibility that UGT2B7 may have the ability to form hetero-oligomer with UGT1A enzymes. Interestingly, bands of hetero-oligomers were also